

Global Biogeochemical Cycles®



RESEARCH ARTICLE

10.1029/2023GB007765

Four Decades of Trends and Drivers of Global Surface Ocean Acidification

Danling Ma¹ , Luke Gregor¹, and Nicolas Gruber¹ 

¹Environmental Physics, Institute of Biogeochemistry and Pollutant Dynamics, ETH Zurich, Zürich, Switzerland

Key Points:

- From 1982 through 2021, surface ocean Ω_{ar} and pH declined at -0.071 ± 0.006 and -0.0166 ± 0.0010 per decade, respectively
- The trends vary spatially, with Ω_{ar} decreasing most strongly in the low latitudes, while pH decreases the most in the high latitudes
- The trends are predominantly caused by rising atmospheric CO_2 , with ocean warming enhancing the pH trend

Supporting Information:

Supporting Information may be found in the online version of this article.

Correspondence to:

N. Gruber,
nicolas.gruber@env.ethz.ch

Citation:

Ma, D., Gregor, L., & Gruber, N. (2023). Four decades of trends and drivers of global surface ocean acidification. *Global Biogeochemical Cycles*, 37, e2023GB007765. <https://doi.org/10.1029/2023GB007765>

Received 8 MAR 2023

Accepted 4 JUL 2023

Author Contributions:

Conceptualization: Danling Ma, Nicolas Gruber

Data curation: Luke Gregor

Formal analysis: Danling Ma, Luke Gregor, Nicolas Gruber

Funding acquisition: Nicolas Gruber

Investigation: Danling Ma, Luke Gregor

Methodology: Danling Ma, Luke Gregor, Nicolas Gruber

Project Administration: Nicolas Gruber

Supervision: Luke Gregor, Nicolas Gruber

Visualization: Danling Ma, Luke Gregor

Writing – original draft: Danling Ma

Abstract The oceans are acidifying in response to the oceanic uptake of anthropogenic carbon dioxide (CO_2) from the atmosphere, yet the global-scale progression of this acidification has been poorly documented so far by observations. Here, we fill this gap and use an updated version of the in situ and satellite observation-based product OceanSODA-ETHZ to determine the trends and drivers of the surface ocean aragonite saturation state (Ω_{ar}) and $\text{pH} = -\log([\text{H}^+])$ (total scale) over the last four decades (1982–2021). In the global mean, Ω_{ar} and pH declined at rates of -0.071 ± 0.006 decade⁻¹ and -0.0166 ± 0.0010 decade⁻¹, respectively, with the errors of the trends largely reflecting the uncertainties in the reconstructed pH and Ω_{ar} fields. These global mean trends are driven primarily by the increase in surface ocean concentration of dissolved inorganic carbon (DIC) in response to the uptake of anthropogenic CO_2 , but moderated by changes in natural DIC. Surface warming enhances the decrease in pH , accounting for $\sim 15\%$ of the global trend. The long-term trends vary substantially across regions and also differ distinctly between pH and Ω_{ar} . The highest trends in pH are found in the high latitudes, while Ω_{ar} decreases the fastest in the low latitudes. These regional differences are primarily a consequence of regional differences in the ability of the surface ocean to take up and buffer the anthropogenic CO_2 . Substantial El Niño-driven interannual variability is superimposed on these trends, with Ω_{ar} showing greater variability than pH , resulting in substantially longer time of emergence for Ω_{ar} .

Plain Language Summary As the ocean takes up human-made carbon dioxide from the atmosphere, it becomes more acidic, that is, its pH is dropping and so is its saturation state of seawater (Ω_{ar}) with respect to aragonite, a type of carbonate mineral. These chemical changes, generally referred to as “Ocean Acidification,” are harming marine organisms. Here, we use an observation-based data set to investigate the trends and drivers of these two important metrics of acidification in the global surface ocean over the last four decades (1982–2021). Our results confirm that pH and Ω_{ar} have been declining across the global ocean and that these trends are predominantly driven by the increase in the surface ocean concentration of dissolved inorganic carbon resulting from the accumulation of human-made CO_2 . We can thus unambiguously demonstrate that it is the human activities-driven emissions of CO_2 that is causing these trends in ocean acidification (OA). We also show that the observed ocean warming enhances the decline in pH . Our study provides, for the first time, a global observation-based quantification of the progression and driving factors of OA, which will help to better understand the impact of OA on marine life.

1. Introduction

The oceans provide a large ecosystem service by taking up roughly a quarter of the CO_2 emitted by anthropogenic activities (Friedlingstein et al., 2022; Gruber et al., 2023; Khaliwala et al., 2013; Sabine et al., 2004), but this comes at a substantial cost, that is, ocean acidification (OA) (Caldeira & Wickett, 2003; Doney et al., 2009; Orr et al., 2005). Although the term “acidification” describes the process by which CO_2 taken up from the atmosphere increases the concentration of hydrogen ions (H^+) in seawater and thereby lowers its pH ($\text{pH} = -\log [\text{H}^+]$), OA encompasses a broader range of chemical changes in seawater. For example, some of the CO_2 that is taken up is titrated away by carbonate ions dissolved in seawater (Sarmiento & Gruber, 2006), reducing the concentration of these ions. This causes the saturation state of calcium carbonate CaCO_3 minerals (Ω), such as that of aragonite (Ω_{ar}), to decline.

Ocean acidification has been the subject of much research in the past two decades since it can severely impact marine life (Doney et al., 2009; R. A. Feely et al., 2004; Gruber et al., 2012; Jiang et al., 2019; Kroeker et al., 2013; Orr et al., 2005). This impact can occur at the level of an individual organism by affecting its physiology or behavioral patterns (Cornwall et al., 2022; Doney et al., 2020; Figuerola et al., 2021; Radford et al., 2021). It

© 2023 The Authors.

This is an open access article under the terms of the [Creative Commons Attribution-NonCommercial License](https://creativecommons.org/licenses/by/4.0/), which permits use, distribution and reproduction in any medium, provided the original work is properly cited and is not used for commercial purposes.

Writing – review & editing: Luke
Gregor, Nicolas Gruber

can also occur all the way up at the scales of communities and ecosystems, for example, by altering population dynamics or by knocking out keystone species and thereby altering community structure (Cornwall et al., 2021; Doney et al., 2020; Hall-Spencer & Harvey, 2019; Harvey et al., 2021). Thus, it is critical that we understand the historical progression and contemporary state of OA across the global ocean. This enables us to track the ocean's chemistry changes while society decarbonizes its economy. However, the ability of the oceanographic community to quantitatively describe the past progression of OA across the global ocean with observations has been remarkably limited. This contrasts with model-based studies which clearly established past and future trends of OA (Bopp et al., 2013; R. A. Feely et al., 2009; Friedrich et al., 2012; Kwiatkowski et al., 2020; Orr et al., 2005; Terhaar et al., 2023).

This lack of observation-based studies of OA trends is in part due to the limited number of historical observations available for the key parameters of OA, that is, $[H^+]$, pH, and Ω_{ar} . For example, seawater pH measurements before 1989 relied primarily on glass electrodes, which involve uncertainties of the order of 0.1 pH units. This is too uncertain to capture the pH alterations induced by OA, rendering these observations unusable. A further complication arises because the pH scale of many earlier records is ambiguous (Jiang et al., 2019). The availability and quality of seawater pH data has improved gradually in the subsequent decades, following the refinement of spectrophotometric pH measurement methods (Byrne & Breland, 1989; Clayton & Byrne, 1993; Dickson, 1993; Jiang et al., 2019). These developments have been greatly aided by efforts such as the Global Ocean Acidification Observing Network (Brewer, 2013; Tilbrook et al., 2019), which supported communities around the world to make high quality measurements, especially in coastal regions. Also, the recent advent of the biogeochemical Argo program with pH sensors has dramatically increased the amount of available data in the last few years, especially in the open seas (Claustre et al., 2020). But the temporal coverage of these data is very limited, preventing an assessment of OA changes over multiple decades. For the saturation state Ω_{ar} or the concentration of the carbonate ion in seawater, the situation is even worse, as they were historically not measured directly. Even though photospectrometric methods to measure the concentration of the carbonate ions have been introduced (Byrne & Yao, 2008) and are increasingly being used, there are too few measurements to assess changes in time.

For these reasons, observation-based OA trend studies have used pH, $[H^+]$, and Ω_{ar} computed from the more frequently measured variables of the ocean carbonate system, namely the partial pressure of CO_2 (pCO_2) and total alkalinity (Alk) (Bates, 2007; Bates et al., 2014; Jiang et al., 2019; Lauvset & Gruber, 2014; Lauvset et al., 2015). Most studies so far have applied this approach for local to regional studies, relying primarily on the data from the few existing long-term time series sites (Bates, 2007; Bates et al., 2014; Olafsson et al., 2010) or the few regions where sufficient observations exist to establish trends directly (Kim et al., 2014; Leseurre et al., 2022; Sutton et al., 2014). These studies unequivocally demonstrated that the ocean is acidifying, revealing highly significant long-term decreases in pH and Ω_{ar} at all sites and regions. But the community lacks an observation-based global-scale analysis that permits researchers to put these local and regional trends into context and also allows them to assess regional differences.

A first attempt to establish global trends in OA based solely on observations was made by Lauvset et al. (2015) who used measured pCO_2 and empirical estimates of Alk to estimate trends in surface ocean pH. They found significant pH decreases in $\sim 70\%$ of all large-scale biomes and a mean rate of decrease of 0.018 ± 0.004 decade⁻¹ for 1991–2011. But their study did not include Ω_{ar} , had insufficient data in several key regions such as the Southern Ocean, required a large amount of spatial aggregation leading to a very low resolution, and was limited in time to two decades. Building on this work and its own synthesis of the data from various time series sites across the world's oceans, the Intergovernmental Panel on Climate Change (IPCC) concluded in its special report on the Ocean and Cryosphere (Bindoff et al., 2019), that “pH in open ocean surface water has changed by a virtually certain range of -0.017 to -0.027 pH units per decade since the late 1980s.” IPCC's Working Group I report in AR6 confirmed, in essence, this very large range for the global mean rate, and also discussed the spatial variability around this mean trend (Canadell et al., 2021). An alternative approach was taken more recently by Jiang et al. (2019) who combined a climatological seawater CO_2 product with model results to obtain trends in the OA parameters. But by relying on a model for establishing the trends, this estimate cannot really be considered observation-based. Most recently, Iida et al. (2021) used observations of Alk and pCO_2 to determine the long-term surface ocean trends in various OA parameters from 1993 to 2018. Differing from previous approaches, they first extrapolated Alk to the global ocean, then used this together with the observed pCO_2 to estimate dissolved inorganic carbon (DIC) at the location and times where pCO_2 was measured, and then extrapolated the resulting DIC field with linear regression models to the globe over the entire recon-

struction period. They suggested that the global mean surface ocean pH had decreased at a rate of -0.018 per decade, and Ω_{ar} at a rate of -0.082 per decade. Their reported uncertainties were very small (± 0.0001 for pH and ± 0.0001 for Ω_{ar}), as they considered only the uncertainty of the trend, thus not considering the uncertainties of the reconstructed pH and Ω_{ar} fields. These unconsidered uncertainties are likely very substantial, since linear regression models are challenged in their ability to correctly capture the time-space variability of DIC. Thus, while there is a pressing need for an observation-based assessment of the trends and drivers of OA on a global scale, the existing analyses are insufficient to fulfill this need. This gap is even more evident when compared to the huge volume of literature on long-term trends and variability in surface ocean pCO₂ (Fay & McKinley, 2013; Fay et al., 2021; Gloege et al., 2022; Landschützer et al., 2014, 2016; Rödenbeck et al., 2015; Tjiputra et al., 2014).

To close this gap, we present a global-scale analysis of the trends and drivers in surface ocean pH, [H⁺], and Ω_{ar} using an updated version of the OceanSODA-ETHZ observation-based product (Gregor & Gruber, 2021). This updated product combines in situ observations and satellite data and covers four decades (1982–2021) at a spatial resolution of $1^\circ \times 1^\circ$, and at monthly resolution in time, and thus provides not only much higher resolution than the previous analysis by Lauvset et al. (2015), but also doubles the length of the analyzed time period. Since the OceanSODA-ETHZ product includes also an estimate of the concentration of DIC, it permits us to analyze also the main drivers for the changes in [H⁺], pH, and Ω_{ar} .

2. Materials and Methods

2.1. OceanSODA-ETHZ Data Set

Our analyses are based on the OceanSODA-ETHZ product (Gregor & Gruber, 2021), which is an observation-based, global gridded data set with monthly data for all parameters of the marine carbonate system parameters at a resolution of $1^\circ \times 1^\circ$. The version used here was updated from the published version by including data for the years 2020 and 2021 and is available through the National Centers for Environmental Information (NCEI, accession 0220059) (Gregor & Gruber, 2023). OceanSODA-ETHZ was derived from the pCO₂ observations provided by Surface Ocean CO₂ Atlas (Bakker et al., 2016) and the Alk observations provided by the Global Ocean Data Analysis Product (Olsen et al., 2016) with a two-step machine learning approach (clustering and regression). This approach maps the observed distribution of pCO₂ and Alk to the global ocean using a range of independent variables as predictors, relying to a substantial degree on satellite observations. We provide here a short description of the main steps and the required input data together with a summary of the uncertainties.

For both pCO₂ and Alk, the observations are first clustered regionally to capture areas of similar variability in the target variable. Thereafter, data in each cluster are fitted using an ensemble of machine-learning approaches. For pCO₂, data are fitted using either a feed-forward neural network or gradient boosted trees, and for Alk, support vector regression was used. The predictors common to Alk and pCO₂ are, sea-surface temperature, sea-surface salinity. For Alk, we further include nutrient variables, and for pCO₂ chlorophyll-a, mixed layer depth, and u and v -wind components. The clustering step is performed 16 times, thus creating an ensemble of 16 members. Each clustering member is slightly different due to the random initialization of the clustering algorithm and the fact that clustering variables are continuous rather than discrete.

Gregor and Gruber (2021) reported that the cluster-regression method estimates the observed open ocean pCO₂ and Alk with global near-zero biases and root mean squared errors of 12 μatm and 13 $\mu\text{mol kg}^{-1}$, respectively. Taking into account also the measurement and representation errors, the total uncertainty was estimated to be about 14 μatm and 21 $\mu\text{mol kg}^{-1}$, respectively. This uncertainty represents the quality with which an individual observation can be estimated by the machine learning approach. This error would largely vanish when computing averages over large regions, since it is of random nature. Thus, in order to estimate the uncertainty of large-scale means, we need to focus on the structural errors in the pCO₂ and Alk estimates, as they do not converge to zero. We estimate these structural errors from the standard deviation of the 16 ensemble members, arriving at global average errors of 5.5 μatm and 4.6 $\mu\text{mol kg}^{-1}$ for pCO₂ and Alk, respectively.

The OceanSODA-ETHZ product used then the mapped pCO₂ and Alk estimates to compute the target quantities of our study, that is, [H⁺], pH, Ω_{ar} , and DIC, by solving the marine carbonate system:

$$\Omega_{ar}, \text{pH}, [\text{H}^+], \text{DIC}, \dots = \text{PyCO2SYS}(p\text{CO}_2, \text{Alk}, T, S, [\text{PO}_4], [\text{Si}(\text{OH})_4]) \quad (1)$$

where PyCO2SYS is the employed software (Humphreys et al., 2020), and where T is sea-surface temperature, S is sea-surface salinity, and where $[\text{PO}_4]$ and $[\text{Si}(\text{OH})_4]$ are the surface ocean concentrations of the nutrients silicic acid and phosphate.

For the dissociation constants of the marine carbonate system, we used the Mehrbach et al. (1973) constants refitted by Dickson and Millero (1987), as this gives the lowest uncertainty when pCO_2 and Alk are used as input (Raimondi et al., 2019). For the remaining choices, we used the default settings of PyCO2SYS, meaning the borate-to-salinity relationship of Uppström (1974) and the sulfate dissociation constants of Dickson et al. (1990). Sea-surface temperature (T) was taken from the National Oceanic and Atmospheric Administration (NOAA) Optimal Interpolation sea surface temperature (SST) V2 High-Resolution Data set (OISSTv2; Reynolds et al., 2007), while sea-surface salinity (S) is a combination of the European Space Agency Climate Change Initiative (ESA-CCI) sea surface salinity (SSS) product for 2010 to 2020 (Boutin et al., 2018) and Simple Ocean Data Assimilation (SODA v3.4.2; Carton et al., 2018) where the ESA-CCI product is not available. Silicic acid and phosphate concentrations were taken from the World Ocean Atlas 2018 (Boyer et al., 2018).

Following many previous studies (e.g., Bates et al., 2014; Lauvset et al., 2015) and the recommendations of the CO_2 handbook (Dickson et al., 2007), we use here the total scale for pH, which includes the contribution of sulfate ions (Dickson, 1993). In contrast, we report for $[\text{H}^+]$ its free concentration, which is equivalent to pH on the free scale (Clayton & Byrne, 1993), that is, without the contribution of the sulfate ions. To highlight this difference, we subsequently denote $[\text{H}^+]$ and pH on the free scale with $[\text{H}^+]_f$ and pH_f , respectively. The use of the free concentration for $[\text{H}^+]$ is motivated by the fact that this is the relevant quantity with regard to biological impacts. Although the differences between pH and pH_f and between $[\text{H}^+]$ and $[\text{H}^+]_f$, respectively, are notable with regard to their absolute values, our choice has no impact on the reported trends, since there are no significant differences between the trends on the different scales. We use the saturation state of Ω_{ar} as the second metric to quantify the evolution of OA (Mucci, 1983; Takahashi et al., 2014). Although aragonite is $\sim 50\%$ more soluble than calcite, the trends for its two saturation states tend to be nearly identical. Results for all other OA relevant properties, such as those of DIC, Alk, pCO_2 , $[\text{CO}_3^{2-}]$, and of the Revelle factor are computed, too, and will be shown in the appendices.

2.2. Analyses of Trends and Their Uncertainties

Trends are calculated on annual averages using ordinary least squares (OLS) regression. The total uncertainty of the trend, σ_{total} was estimated by considering two main sources of errors, that is, (a) the error of the trend, σ_{trend} , and (b) the error of the underlying data, σ_{data} . This gives:

$$\sigma_{\text{total}} = \sigma_{\text{trend}} + \sigma_{\text{data}}, \quad (2)$$

where we add these two errors linearly, since we do not know how independent the two error sources are.

The error of the trend, σ_{trend} , is estimated from the square root of the variance of the slope coefficient. This coefficient is calculated from the covariance matrix of the OLS solution: $(\mathbf{X}'\mathbf{X})^{-1} \cdot \text{MSE}$, where \mathbf{X} is a matrix of the predictors and MSE is the mean squared error of the fit.

The error of the data, σ_{data} , was estimated from the spread of the ensemble of estimates that we have available in the OceanSODA-ETHZ product. As explained above, this error is non-random in nature and thus is a better representation of the uncertainty associated with the machine-learning-based estimates compared to the use of root mean squared errors vis-a-vis the observations. While we can use this ensemble spread right away for pCO_2 and Alk, we need to propagate these uncertainties to the other computed parameters of the marine carbonate system. To this end, we first created a total of 64 ensemble members by randomly selecting one of the 16 ensemble members for pCO_2 and one of the 16 for Alk without repetition and then recomputing all derived variables from this combination. In the global mean, this resulted in standard deviations across the ensemble of about 0.014 and 0.0022 for Ω_{ar} and pH, respectively. The long-term trends were then calculated for each ensemble member and for each $1^\circ \times 1^\circ$ pixel. The standard deviation is taken across all 64 ensemble members for each pixel, resulting in a map of the standard deviations of the trend. These pixel-level standard deviations are then averaged globally and for each region (area-weighted).

To assess the robustness of this approach to compute the trend uncertainty, we compare it with an independent ensemble approach, which is available for pCO_2 . Concretely, we take advantage of the ensemble of six pCO_2

estimates available in the Fay et al. (2021) SeaFlux product, which has been constructed by independent methods ranging from neural networks to linear regression models. We consider, however, only 5 of the 6 available products, since we excluded the JMA-MLR product of Iida et al. (2021). This is because this product has a $p\text{CO}_2$ trend that is outside the three-times interquartile range of the other products and thus would have skewed our results.

2.3. Driver Decomposition of Trends

To quantify and understand the drivers of the trends in Ω_{ar} and $[\text{H}^+]_F$, we decompose them into contributions from trends in the underlying drivers, that is DIC, Alk, T, and freshwater (FW). The freshwater driver includes both the direct effect of changes in salinity on Ω_{ar} and pH, as well as the indirect effect caused by changes in the surface ocean DIC and Alk due to the net freshwater balance (Landschützer et al., 2018; Lovenduski et al., 2007). To this end, we remove the freshwater component from the DIC and Alk driver by normalizing these two parameters to a constant salinity of 34.5 (Landschützer et al., 2018; Sarmiento & Gruber, 2006). The resulting quantities are denoted by sDIC and sAlk. We further decompose sDIC into an anthropogenic and a natural component, that is, $\text{sDIC} = C_{ant} + C_{nat}$ (Gruber et al., 2023; McNeil & Matear, 2013). C_{ant} captures the changes in sDIC driven solely by the anthropogenic increase in atmospheric CO_2 and the resulting uptake of anthropogenic CO_2 by the surface ocean. The C_{nat} component represents the changes in sDIC driven by changes in circulation, solubility, and biology.

Neglecting the contributions from other minor drivers such as nutrients, we thus decompose the variations in the trends of Ω_{ar} and $[\text{H}^+]_F$ to five main driving components: anthropogenic sDIC (C_{ant}), natural sDIC (C_{nat}), sAlk, temperature (T) and freshwater (FW). Considering only the first-order terms of a Taylor expansion and using the product rule, this gives the rate of change of Ω_{ar} :

$$\frac{d\Omega_{ar}}{dt} = \sum_{X=[C_{ant}, C_{nat}, sAlk, T, FW]} \left(\underbrace{\frac{d\omega_X}{dt} \cdot \Omega_{ar} \cdot \Delta X}_{\text{change in sensitivity}} + \underbrace{\omega_X \cdot \frac{d\Omega_{ar}}{dt} \cdot \Delta X}_{\text{mass effect}} + \underbrace{\omega_X \cdot \Omega_{ar} \cdot \frac{d\Delta X}{dt}}_{\text{change in driver}} \right), \quad (3)$$

where X is one of the five drivers, ΔX is the change in the driver (from 1982 through 2021), and ω_X is the relative sensitivity of Ω_{ar} to each driver, that is, $\omega_X = 1/\Omega_{ar} \cdot \partial\Omega_{ar}/\partial X$. Note that this definition of ω_X differs from that of Egleston et al. (2010) who defined it as the sensitivity of X to Ω_{ar} . The time derivatives on the right-hand side of Equation 3 are determined from the slopes of the linear regressions.

The same decomposition is applied for $[\text{H}^+]_F$, that is,

$$\frac{d[\text{H}^+]_F}{dt} = \sum_{X=[C_{ant}, C_{nat}, sAlk, T, FW]} \left(\underbrace{\frac{d\beta_X}{dt} \cdot [\text{H}^+]_F \cdot \Delta X}_{\text{change in sensitivity}} + \underbrace{\omega_X \cdot \frac{d[\text{H}^+]_F}{dt} \cdot \Delta X}_{\text{mass effect}} + \underbrace{\omega_X \cdot [\text{H}^+]_F \cdot \frac{d\Delta X}{dt}}_{\text{change in driver}} \right), \quad (4)$$

where β_X is the relative sensitivity of $[\text{H}^+]_F$ to each driver X , that is, $\beta_X = 1/[\text{H}^+]_F \cdot \partial[\text{H}^+]_F/\partial X$. The relative sensitivities β and ω are calculated with the PyCO2SYS program (Humphreys et al., 2020; Lewis et al., 1998) for each grid point, using the long-term average conditions as input. The temperature sensitivities are assumed to be constant for the entire range of DIC and Alk, with a value of $0.0052^\circ\text{C}^{-1}$ for Ω_{ar} and a value of $0.0354^\circ\text{C}^{-1}$ for $[\text{H}^+]_F$.

The surface ocean concentration of C_{ant} and its rate of change is estimated by assuming that surface ocean DIC increases proportionally with the increase in atmospheric CO_2 (Gruber et al., 2023). We determine this proportionality by computing first the amount of C_{ant} the surface ocean would have if it had remained in transient equilibrium with the overlying atmosphere, that is, the C_{ant}^{eq} component. We then adjust this component to account for the fact that the increase in surface C_{ant} is increasingly delayed, leading to a growing disequilibrium term, that is, C_{ant}^{dis-eq} , which is also proportional to the rise in atmospheric CO_2 (see Matsumoto and Gruber (2005) and Gruber et al. (2019) for a more in-depth discussion). Concretely, C_{ant} is given by: $C_{ant} = C_{ant}^{eq} - C_{ant}^{dis-eq}$. We determine C_{ant}^{eq} at each surface location by evaluating Equation 1 whereby the in situ $p\text{CO}_2$ is replaced with atmospheric CO_2 from the NOAA marine boundary layer product (Dlugokencky et al., 2021). We take the disequilibrium term

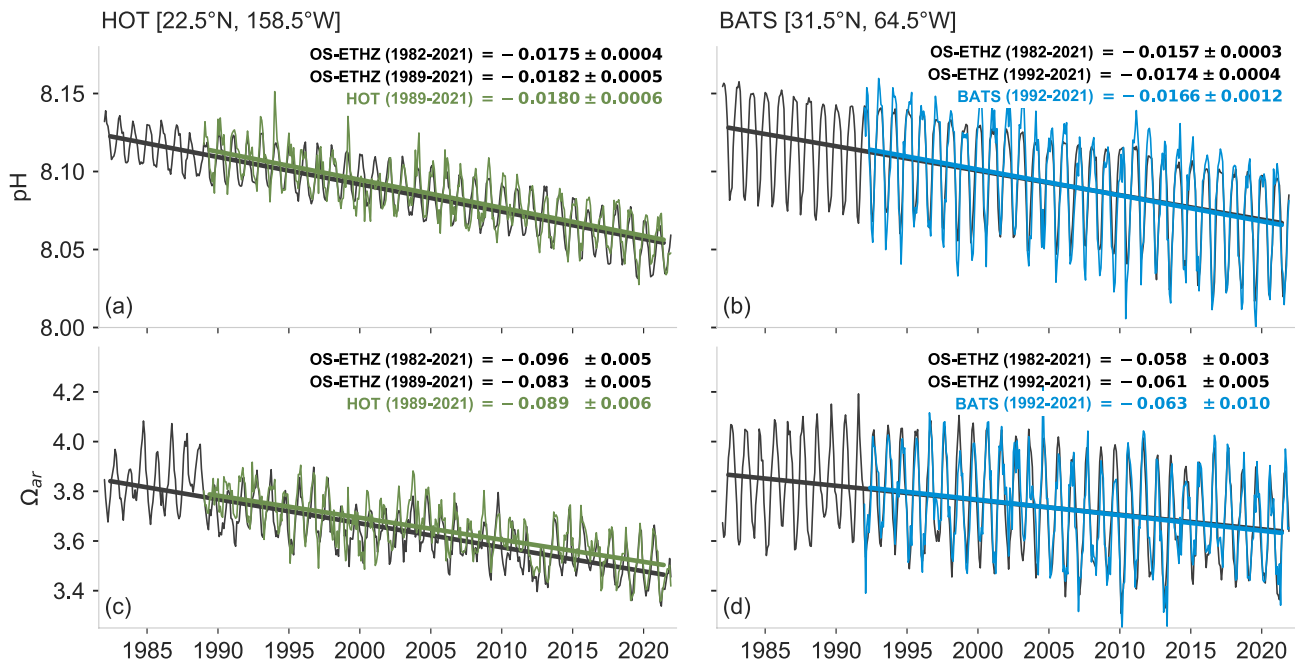


Figure 1. Evaluation of trends in the OceanSODA-ETHZ product with observations from (a, c) the Hawaii Ocean Time-series (Dore et al., 2009) in the North Pacific (left column) and the Bermuda Atlantic Time series Study in the North Atlantic (Bates & Johnson, 2020; Bates et al., 2014) (b, c). Shown are the OceanSODA-ETHZ estimates and the surface ocean observations for (a, b) pH (total scale) and for (c, d) Ω_{ar} . The lines represent the results of the trend analyses on the basis of ordinary least squares linear regressions. The observation data for the time series sites were computed from the reported dissolved inorganic carbon and Alk measurements.

C_{ant}^{dis-eq} from a hindcast simulation with the ocean component of the Community Earth System Model (Clement & Gruber, 2018; Hauck et al., 2020). The trend in the natural component, C_{nat} , is computed by subtracting C_{ant} from sDIC, that is, $C_{nat} = sDIC - C_{ant}$, whereby all components are salinity normalized to 34.5.

2.4. Time of Emergence

The Time of emergence (ToE) is defined as the time it takes for a signal to arise from the “noise” of natural climate variability (Keller et al., 2014):

$$\text{ToE} = N/S, \quad (5)$$

where N is the “noise,” estimated from the standard deviation of the detrended monthly data, and S is the “signal,” that is, the annual trend. We thus take here the perspective that the ToE is a measure when the system of interest goes outside the range of prior (seasonal and interannual) variability, a metric that is particularly relevant to marine organisms. The TOE has units of years.

3. Results and Discussions

3.1. Evaluation

The rate of pH change estimated from OceanSODA-ETHZ generally agrees well with the reported rates from time series sites around the globe (Table S1 in Supporting Information S1). However, many time series sites have reported trends over much shorter periods, typically, only two decades, making the comparisons less robust owing to a stronger imprint of shorter variability on the long-term trends. We thus focus the evaluation of our trend estimates with those stemming from the longest-running (>30 years) and best-sampled time series sites in the ocean, namely the Hawaii Ocean Time-series (HOT) (Dore et al., 2009) in the North Pacific (22.5°N, 158.5°W) and the Bermuda Atlantic Time series Study (BATS) in the North Atlantic (31.5°N, 64.5°W) (Bates & Johnson, 2020; Bates et al., 2014) (Figure 1). This evaluation is particularly insightful since the data from these two time series sites were not used for the training of the machine-learning algorithm in OceanSODA-ETHZ. Neither site measured pH or Ω_{ar} , but DIC and Alk, from which we computed pH and Ω_{ar} following the same procedures as used

for OceanSODA-ETHZ. We also recomputed the long-term trends in order to ensure maximum comparability with our estimates. To this end, we first deseasonalized the data from the time series stations using a harmonic fit (Gruber et al., 2002) and then computed the trend in the same manner as done for OceanSODA-ETHZ.

For BATS and the period covered by this site, that is, 1992–2021, we compute for OceanSODA-ETHZ a decadal rate of change for pH of $-0.0174 \pm 0.0004 \text{ decade}^{-1}$, statistically indistinguishable from the trend we determined from the reported time series data (Figure 1). By including data from the nearby Station “S” (Gruber et al., 2002), Bates and Johnson (2020) were able to extend this record back in time, reporting for 1983–2020 a slightly more negative trend of $-0.0190 \pm 0.0010 \text{ decade}^{-1}$ (Table S1 in Supporting Information S1), a bit more negative than our estimate for the same period (-0.0157 ± 0.0003) (Figure 1). The trends for Ω_{ar} are slightly more different, but still in agreement within the respective uncertainties. While our estimate for the period 1992–2021 of $-0.061 \pm 0.005 \text{ decade}^{-1}$ is again statistically indistinguishable from the trend we computed from the time series data ($-0.063 \pm 0.010 \text{ decade}^{-1}$), Bates and Johnson (2020) found for the combined Station “S” and BATS sites over the 1983–2020 period a trend of $-0.090 \pm 0.010 \text{ decade}^{-1}$, which is quite a bit more negative than ours (Figure 1, Table S1 in Supporting Information S1). However, we note that Bates and Johnson (2020) used a different method to estimate trends, such that some of the differences are also the result of methodological differences.

Our pH trend estimate for the HOT site (1989–2021) of $-0.0182 \pm 0.0005 \text{ decade}^{-1}$ is nearly identical to that we computed from the reported time series data ($-0.0180 \pm 0.0006 \text{ decade}^{-1}$). But, as was the case at BATS, there is lesser agreement on the trend in Ω_{ar} . For OceanSODA-ETHZ, we find a trend of $-0.083 \pm 0.005 \text{ decade}^{-1}$, while for the time series data, the trend amounts to $-0.089 \pm 0.006 \text{ decade}^{-1}$.

The evaluation of the trends at the other time series sites (Table S1 in Supporting Information S1), often of much shorter duration, confirms the overall excellent agreement. But this comparison also suggests that the OceanSODA-ETHZ has a slight tendency for underestimating long-term trends, especially for Ω_{ar} . This could be a consequence of the cluster-regression approach that we employed in ensemble mode to create OceanSODA-ETHZ, as this machine-learning method tends to suppress variations and trends (Gregor & Gruber, 2021). Still, these evaluations suggest that OceanSODA-ETHZ reproduces the observed long-term trends at the time series stations with high fidelity, giving us confidence in the use of this product to assess long-term trends in OA across the global ocean (Chau et al., 2022).

3.2. Long-Term Trends

The temporal evolution of the reconstructed global surface mean Ω_{ar} , pH, and $[\text{H}^+]_F$ from the OceanSODA-ETHZ product confirms the expected strong trends induced by OA over the four decades from 1982 through 2021 (Figure 2). Averaged over the global ice-free ocean, surface Ω_{ar} decreased by nearly 10% over these four decades, and pH experienced a drop of ~ 0.06 units. At the same time, $[\text{H}^+]_F$ increased proportionately by slightly more than 1 nmol kg^{-1} . This translates into highly significant average trends of $-0.071 \pm 0.006 \text{ decade}^{-1}$ for Ω_{ar} ($R^2 = 0.98$; $p \ll 0.01$) and $-0.0166 \pm 0.0010 \text{ decade}^{-1}$ for pH ($R^2 = 0.99$; $p \ll 0.01$) (see Table 1). For $[\text{H}^+]_F$ the average rate of increase amounts to $0.250 \pm 0.016 \text{ nmol kg}^{-1} \text{ decade}^{-1}$. In Table 1 we report also the trends for a range of additional parameters of the surface ocean carbonate system, such as surface ocean pCO_2 and the Revelle factor. In Table S2 of the Supporting Information S1, we provide the trends of these variables for a large number of biogeochemical provinces (Fay & McKinley, 2014). The global trends are rather robust and not sensitive to the choice of the exact beginning or ending years. For example, shortening the record to 30 years and computing the trends by shifting the beginning year from 1982 to 1992 yields variations in the trends of $< 7\%$.

The uncertainties of the trends reported above and in the tables (Table 1 and Table S2 in Supporting Information S1) reflect the total uncertainties (σ_{total}). We computed those by summing the errors associated with the determination of the regression slope, that is, σ_{trend} , and the errors induced by systematic errors associated with the underlying data, that is, σ_{data} (see Equation 2). We find that the data-related errors are, on average, about 3–4 times larger than the trend-related errors, thus accounting for about 80% of the total uncertainty (Figure S3 in Supporting Information S1). Thus, an accurate estimation of the data-related errors is key for estimating the total uncertainty of the trend in the OA-related parameters. For estimating these data-related errors, we relied on a commonly used ensemble approach, taking advantage of the ensemble nature of OceanSODA-ETHZ. However, since all our ensembles are based on the same statistical approach, they might underestimate the data-related errors. We thus tested our approach by comparing its results with those obtained from a full ensemble of pCO_2

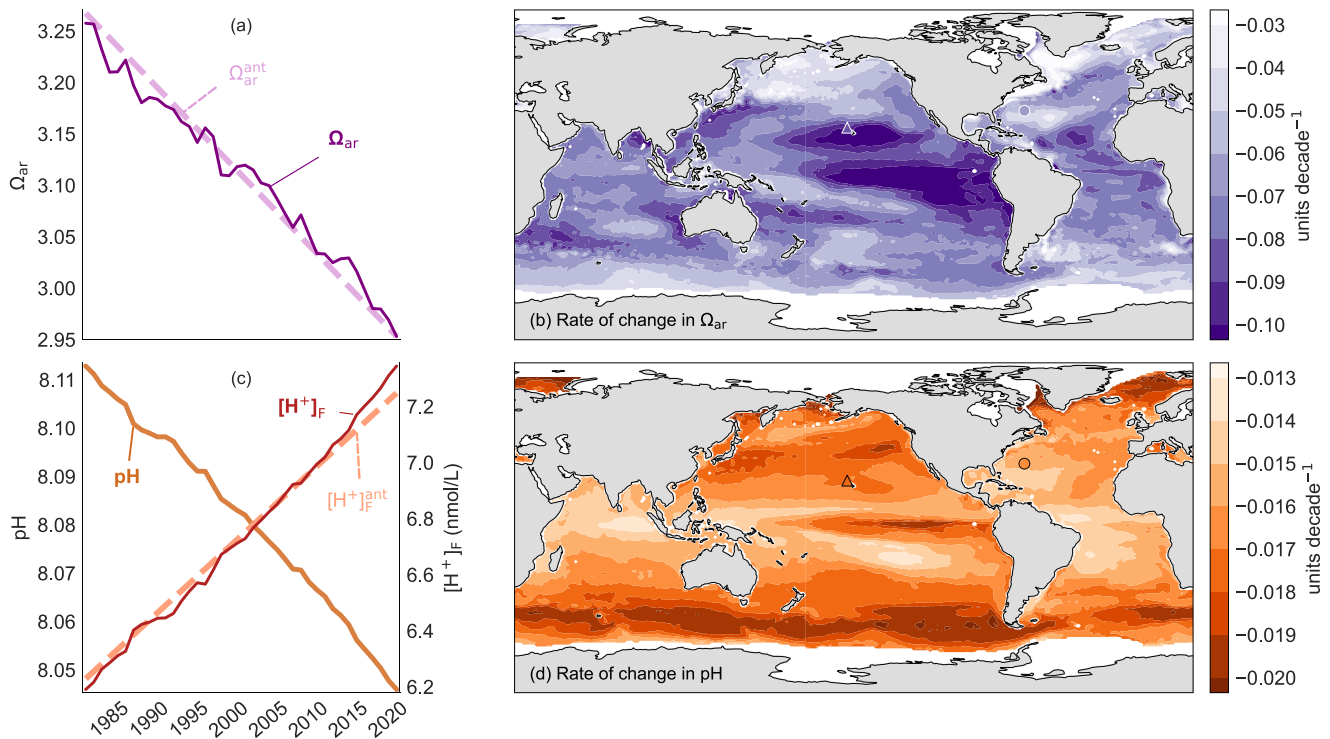


Figure 2. Temporal and spatial structure of the long-term trends in global aragonite saturation state (Ω_{ar}), pH, and $[H^+]_F$ from 1982 to 2021 using OceanSODA-ETHZ data (Gregor & Gruber, 2021). (a) Global area-weighted trend for Ω_{ar} (solid line), along with the estimated anthropogenic trend (dashed line) based on the estimated increase in C_{ant} . (b) Global map of the 40-year average trend of Ω_{ar} , expressed as a trend per decade. (c) As (a) but for pH (left axis) and $[H^+]_F$ (right axis) with the estimated anthropogenic increase being shown for the latter only. (d) As (b), but for pH. Note that the global average trends plotted in (a) and (c) are computed over the colored areas shown in (b) and (d), representing 96% of the global sea-ice-free surface area. The triangle and circle in (b) and (d) indicate the locations of the two time series Hawaii Ocean Time-series and Bermuda Atlantic Time series Study used to evaluate the OceanSODA-ETHZ product in detail (see Figure 1). The uncertainties of the estimated annual mean fields are ± 0.014 for Ω_{ar} and ± 0.0022 for pH, that is, too small to be plotted.

estimates in the SeaFlux product of Fay et al. (2021). Across the 5 retained ensemble members in SeaFlux, we find for pCO_2 a trend of $16.7 \pm 1.5 \mu atm decade^{-1}$ (1990–2018), while that estimated through our approach is $17.0 \pm 0.8 \mu atm decade^{-1}$ for the same period (see Figure S3 in Supporting Information S1). Thus, there might be indeed a tendency for our uncertainty estimates to be biased low. But lacking a standardized methodology

to estimate such uncertainties, we accept our total uncertainty estimates of slightly less than $\pm 10\%$ as our best estimate.

Our global mean surface pH trend supports the trend estimated by Lauvset et al. (2015) of $-0.018 \pm 0.004 decade^{-1}$ for the period 1991 through 2011, we can now provide a much more accurate estimate covering 96% of the global sea-ice-free surface ocean as opposed to the 70% coverage available to Lauvset et al. (2015). Our estimate permits us also to reduce the range given by IPCC (Bindoff et al., 2019), that is, -0.017 to $-0.027 decade^{-1}$, by nearly tenfold. Our global pH trend matches also well those given by a range of Earth System Models (Kwiatkowski et al., 2020). Finally, our trend is also fully consistent with that reported by Iida et al. (2021) of $-0.018 \pm 0.0001 decade^{-1}$, although, we provide a much more thorough and robust uncertainty estimate. Our Ω_{ar} trend is not as strong as that reported by Iida et al. (2021) ($-0.082 \pm 0.001 decade^{-1}$), but if they had accounted for the uncertainty in their product, it is likely that our two estimates also would not be significantly different.

Spatially, there are large variations in the rates of the Ω_{ar} and pH declines over the past four decades (Figures 2b and 2d) (see also Tables S3 and S4 in

Table 1
Mean Values and Global Long-Term Trends of a Suite of Parameters of the Surface Ocean Carbonate System for the Period 1982 Through 2021

Variable	Unit	Mean value	Trend \pm uncertainty (decade ⁻¹)
Ω_{ar}	(–)	3.11	-0.071 ± 0.006
Ω_{calc}	(–)	4.75	-0.111 ± 0.009
pH	(–)	8.08	-0.0166 ± 0.0010
$[H^+]_F$	(nmol kg ⁻¹)	6.74	0.250 ± 0.016
DIC	($\mu mol kg^{-1}$)	2,025	8.3 ± 0.8
pCO_2	(μatm)	359	16.6 ± 1.0
Revelle factor, γ_{DIC}	(–)	10.5	0.156 ± 0.011
$[CO_3^{2-}]$	($\mu mol kg^{-1}$)	198	-4.6 ± 0.4

Note. All trends are computed from annual data of the OceanSODA-ETHZ product and are given per decade. The uncertainties contain both the errors of the trend slope (σ_{trend}) and the errors of the data (σ_{data}) (see Equation 2).

Supporting Information S1). For Ω_{ar} , the largest trends are found in the tropical and subtropical Pacific Ocean, including the eastern tropical Pacific region (Figure 2b), with rates of Ω_{ar} decreases that are, on average, 50% higher than in the global mean. In contrast, Ω_{ar} drops much less in the North Pacific and North Atlantic and parts of the Southern Ocean. Here, rates tend to be only half those of the global mean. This gives overall a factor of four difference in rates across the global ocean, highlighting the importance of the regional perspective when investigating OA.

The spatial distribution of the rate of decline in pH tends to be the mirror image of that of Ω_{ar} (Figure 2d), although the range of the trends is smaller. The highest rates of decline are found in the Southern Ocean and in the high latitudes of the North Atlantic and North Pacific. Rates are here, expressed in the logarithmic pH units, about 15% higher than in the global mean. The lowest rates of change are found in the subtropical gyres, with rates that are about 25% lower than the global mean. Another striking pattern is that the trends in the Pacific tend to be larger than those in the Atlantic for the same latitude. A region that breaks the mirror image, that is, where both Ω_{ar} and pH show large changes, is a small equatorial band in the eastern and central Pacific.

The spatial distribution of the trends in the other parameters of the surface ocean carbonate system (shown in Figure S5 in Supporting Information S1) fall into a set of trend pattern that resembles the trends of pH ($[H^+]$, pCO_2 , Revelle factor), that is, highest rates of change in the high latitudes or into a set of pattern that resembles the trends of Ω_{ar} (carbonate ion concentration, $[CO_3^{2-}]$), that is, highest rates of change in the low latitudes. This is largely a consequence of the relationships of these parameters with each other, for example, the carbonate ion concentration is a direct determinant of Ω_{ar} , and pCO_2 is highly correlated with pH and $[H^+]$. The similarity of the trend pattern of the Revelle factor with that of pH is, however, initially surprising, since as a metric of the buffering capacity of the surface ocean, its value tends to be related to the concentration of the carbonate ion (Sarmiento & Gruber, 2006). This can be resolved by considering that the Revelle factor scales with the inverse of $[CO_3^{2-}]$, such that we also expect the trend of the Revelle factor to scale with the inverse of the trend of $[CO_3^{2-}]$. This results in the high latitudes having the largest trends in the Revelle factor, since this is where the trend in $[CO_3^{2-}]$ is the smallest.

The distinct spatial variations of the rates of change of OA had been discussed in the literature only sparingly so far. Lauvset et al. (2015) also found trends that varied considerably across the analyzed biomes, but given the large uncertainties of their regional trends, they refrained from discussing them in detail. They did point to the systematic differences between the Atlantic and Pacific, however. A systematic difference we can confirm here. In its global assessment, IPCC AR6 (Canadell et al., 2021) discussed the regional differences as well, pointing out, for example, that the central and eastern upwelling zones of the Pacific exhibited a faster pH decline of -0.022 to -0.026 decade $^{-1}$ (see also Sutton et al. (2014)) compared to the western tropical Pacific, where the trends are only in the range of -0.010 to -0.013 decade $^{-1}$ (see also Ishii et al. (2020)). This strong east-west gradient in the tropical Pacific is fully confirmed by our results (Figure 2d). IPCC AR6 further suggested for the subtropical gyres pH trends ranging from -0.016 to -0.019 decade $^{-1}$, which is a smaller range than that we find (-0.013 to -0.019 decade $^{-1}$). In contrast, IPCC AR6 suggests subpolar latitudes values ranging from -0.003 decade $^{-1}$ to -0.026 decade $^{-1}$, while our work suggests a substantially smaller range (-0.017 to -0.020 decade $^{-1}$). We interpret these differences to be primarily the result of the relatively small number of time series sites that were used by the IPCC for their assessment. We are not aware of any study that investigated the spatial pattern of the trend in Ω_{ar} in a systematic manner, although IPCC AR6 (Canadell et al., 2021) mentioned the regional differences.

3.3. Drivers of the Long-Term Trends

The driver decomposition Equations 3 and 4 confirms the expectation that the majority of the decreasing trend in Ω_{ar} and increasing trend in $[H^+]_F$ is driven by the anthropogenic increase in atmospheric pCO_2 causing an increase in surface ocean C_{ant} (dashed lines in Figures 2a and 2c). This conclusion is in line with IPCC's assessments (Bindoff et al., 2019; Canadell et al., 2021) as well as with prior work (Lauvset et al., 2015; Lauvset & Gruber, 2014). However, hidden behind the dominant role of C_{ant} are substantial and relevant contributions from the other drivers. A first indication of this comes from the global trend in Ω_{ar} in Figure 2a, which is decreasing somewhat less rapidly than expected from the anthropogenic trend alone (compare dashed with solid lines). The estimated trend based on the increase in surface ocean C_{ant} amounts to -0.087 decade $^{-1}$ (Table S4 in Supporting Information S1), about 20% larger than the observed trend of -0.071 decade $^{-1}$. This differs markedly from the trends in pH and $[H^+]_F$, which agree remarkably well with the anthropogenic trend (Table S4 in Supporting

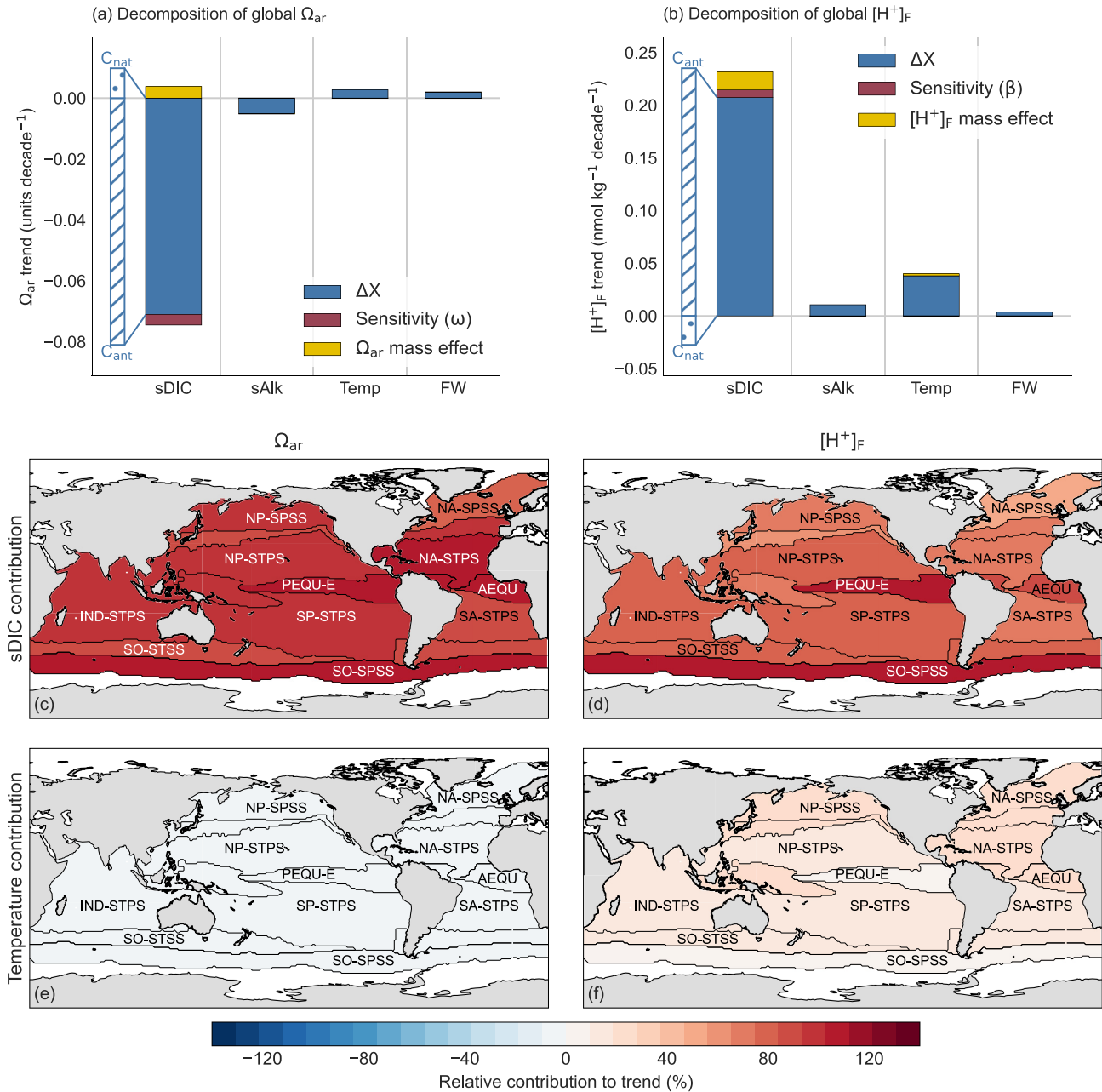


Figure 3. Decomposition of the global mean rate of change of (a) Ω_{ar} and (b) $[H^+]_F$ over the period 1982–2021 into their main drivers following Equations 3 and 4 in the main text. The considered drivers are: salinity normalized dissolved inorganic carbon (sDIC) separated into its anthropogenic CO_2 (C_{ant}) and natural CO_2 (C_{nat}) components, sea surface temperature (SST), salinity normalized alkalinity (sAlk), and freshwater (FW). Also shown for each driver are the contributions of the three mechanisms: change in the driver sensitivity (blue), change in the carbonate system variable (yellow), and change in the driver itself (red). Also shown here are maps showing the relative contribution of (c) sDIC to the rate of change of Ω_{ar} , (d) sDIC to the trend of $[H^+]_F$, (e) SST to the trend in Ω_{ar} , and (f) SST to the trend in $[H^+]_F$ aggregated to each biome.

Information S1). A second indication comes from the full driver decomposition in Figures 3a and 3b, which shows that changes in natural CO_2 , temperature, and to a somewhat smaller degree also sAlk, contribute substantially to the trends, especially for $[H^+]_F$. We discuss these two indications in sequence.

According to our decomposition, the main reason for the smaller-than-expected long-term trend in Ω_{ar} is the substantial compensation by natural CO_2 (C_{nat}) (Figure 3a). This means that in the OceanSODA-ETHZ product, the concentration of sDIC is not increasing as fast as predicted from the increase in anthropogenic CO_2 (C_{ant})

because of a loss in C_{nat} (see also Figure S1 in Supporting Information S1). Thus this smaller-than-expected increase in sDIC causes a lower rate of decrease of the carbonate ion concentration predicted from the increase in C_{ant} alone, hence causing a lower rate of decrease of Ω_{ar} . Changes in sAlk are relatively minor (generally less than $4 \mu\text{mol kg}^{-1}$ over the entire 4 decades, see Figure S5b in Supporting Information S1), and its small global decrease enhances the decrease in Ω_{ar} (Figure 3a and Table S4 in Supporting Information S1). In contrast, warming and the freshwater component act to compensate for the anthropogenic CO_2 -driven decrease in Ω_{ar} , but their contribution is small (Figure 3a). Similarly, the mass effect slows the rate of decrease of Ω_{ar} . In summary, the contribution of the non-sDIC components is small, so that it is the decrease in C_{nat} , that is, the reduction in the concentration of natural CO_2 in the surface ocean that causes global mean Ω_{ar} to decrease less rapidly than predicted from the rise in atmospheric CO_2 alone. A similar reduction of C_{nat} in the surface ocean has recently been identified by Keppler et al. (2023) on the basis of machine-learning-based reconstructions of the spatiotemporal evolution of DIC. They suggest that this reduction at the surface is compensated by an increase at depths below 200 m, such that the total ocean inventory of C_{nat} did not change.

The decomposition of the trends for $[\text{H}^+]_F$ reveals a different picture (Figure 3b). While the strong increase in $[\text{H}^+]_F$ driven by C_{ant} is also compensated by the decrease in C_{nat} , the other components, are contributing substantially to the driving up of the trend in $[\text{H}^+]_F$ (Figure 3b). The most important driver is temperature, which contributes $\sim 15\%$ to the rate of increase in $[\text{H}^+]_F$. But also the $[\text{H}^+]$ mass effect and the increased sensitivity contribute to the rise in $[\text{H}^+]_F$. Taken together, a different balance emerges for the trend in $[\text{H}^+]_F$ compared to that of Ω_{ar} . For $[\text{H}^+]_F$, the slowing trend induced by the loss of C_{nat} is nearly entirely compensated for by the accelerating trend induced by surface ocean warming, so that the overall trend is remarkably close to that predicted by C_{ant} alone. In other words, the loss of C_{nat} tends to mask the quite substantial accelerating contribution of ocean warming on the trend of $[\text{H}^+]_F$. Temperature plays a much less important role in driving trends of Ω_{ar} , because the temperature effects on the dissociation constants relevant for the computation of Ω_{ar} tend to cancel each other.

Thus for both trends, we find an important modification of the purely anthropogenic CO_2 trend by surface ocean warming and the loss of C_{nat} , albeit with different relative roles. Before we discuss this finding further, we need to ensure that it is robust. This is especially critical since we estimate the trend in C_{nat} by difference from the trend in sDIC and C_{ant} . Of particular concern is our estimate of the disequilibrium component, which we use to adjust the equilibrium estimate of C_{ant} for the fact that even in the absence of any climate variability surface ocean sDIC is not following perfectly the increase in atmospheric CO_2 owing to the slowness of air-sea gas exchange and limited surface residence times (Matsumoto & Gruber, 2005). Globally, the mean air-sea disequilibrium is actually very well-constrained since it is directly related to the oceanic uptake of anthropogenic CO_2 , which is known to be within about $\pm 15\%$ on the basis of multiple approaches (DeVries, 2014; Gruber et al., 2019, 2023; Hauck et al., 2020; Mikaloff Fletcher et al., 2006; Sabine et al., 2004). It turns out that even adopting an uncertainty for the air-sea disequilibrium of $\pm 30\%$ would not alter our conclusion that C_{nat} has decreased over the last four decades. We thus consider this conclusion as robust.

The diagnosed loss of C_{nat} from the surface ocean slowing down the rate of change of Ω_{ar} and $[\text{H}^+]_F$ can also be rationalized from a process perspective, especially since it is connected to surface ocean warming. First, one expects a loss of C_{nat} from the surface ocean in response to the reduced CO_2 solubility associated with surface warming (Weiss, 1974). Second, upper ocean warming has been linked to the observed increase in upper ocean stratification (Sallée et al., 2021), which tends to make the biological pump more efficient, causing a reduction in surface ocean DIC (Sarmiento & Gruber, 2006).

The important contribution of ocean warming to the long-term trend in $[\text{H}^+]_F$ becomes also very clear when investigating this decomposition on a regional basis, here shown just for the contribution from sDIC, that is, the sum of natural and anthropogenic CO_2 (Figures 3c and 3d), and for temperature (Figures 3e and 3f). While the contribution of warming to the trend in Ω_{ar} is less than a few percent, this number is about 8% for $[\text{H}^+]_F$, on average. The highest contributions are found in the North Atlantic and the western Pacific, that is, the regions that experienced the highest rates of surface warming in the last few decades (Johnson & Lyman, 2020).

Still, the majority of the long-term trend for both $[\text{H}^+]_F$ and Ω_{ar} across all regions stem from the increase in sDIC (Figures 3c and 3d). This means that the distinct spatial differences in the rates of change in $[\text{H}^+]_F$ and Ω_{ar} seen in Figure 2 and shown as zonal means in Figures 5c and 5f are caused by the product of the spatial pattern of the sensitivities β_{DIC} and ω_{DIC} , respectively, with the trend in C_{ant} , whose spatial pattern is given by the inverse of the sensitivity γ_{DIC} (Eggleston et al., 2010) (Figure 4). This means that one can understand the trends in $[\text{H}^+]_F$ and Ω_{ar}

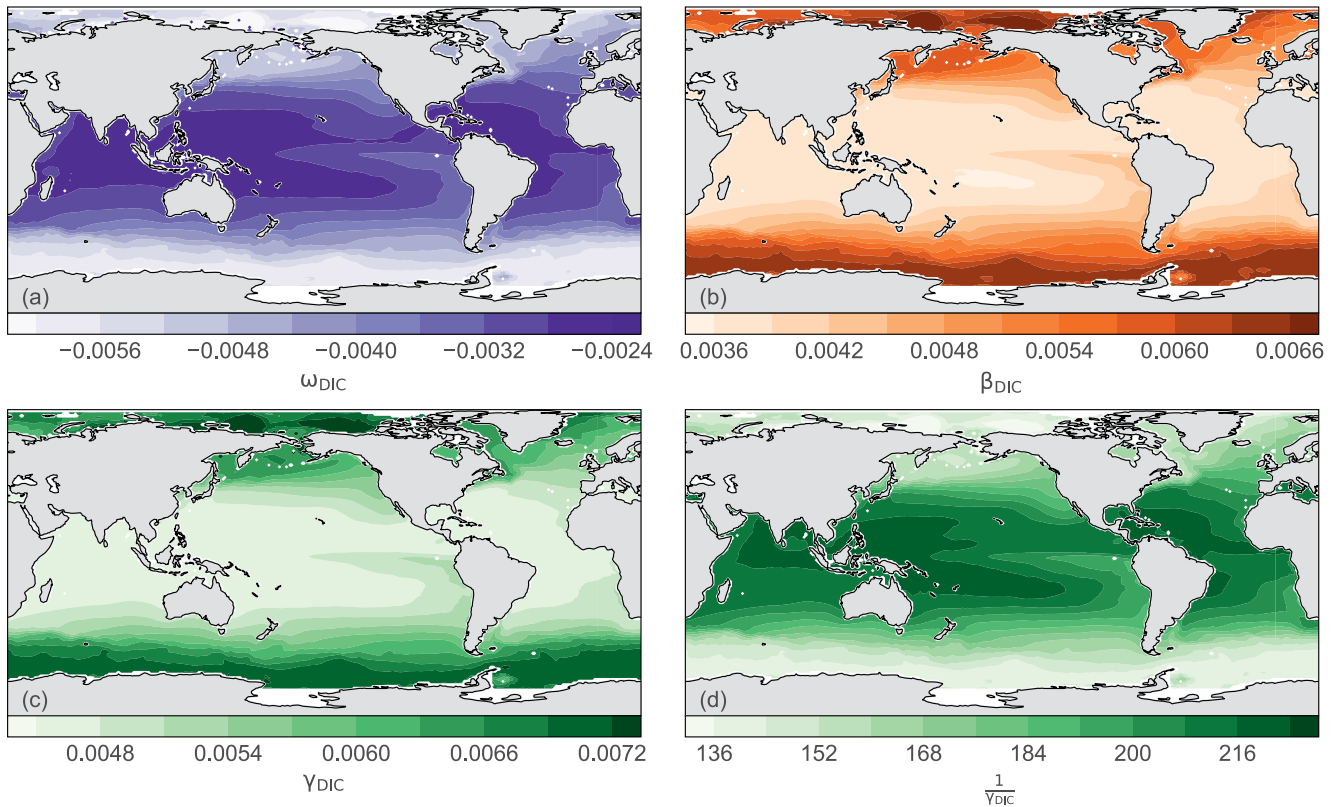


Figure 4. Maps depicting the average sensitivities of parameters of the surface ocean carbonate system to changes in dissolved inorganic carbon. (a) The sensitivity of Ω_{ar} , that is, ω_{DIC} (b) the sensitivity of $[H^+]_F$, that is, β_{DIC} , (c) the sensitivity of pCO_2 , that is, γ_{DIC} . (d) The inverse of the pCO_2 sensitivity, that is, $1/\gamma_{DIC}$. The sensitivities represent the average for the period 1982–2021.

as being proportional to the ratio of β_{DIC}/γ_{DIC} and $\omega_{DIC}/\gamma_{DIC}$, respectively (see also Orr (2011) for a detailed discussion). All of these sensitivities are reflections of how well the surface carbonate chemistry is able to buffer the increase in surface ocean CO_2 , which depends on temperature, and especially the ratio of DIC and Alk (Egleston et al., 2010; Sarmiento & Gruber, 2006).

In the case of the trends in $[H^+]_F$ (and pH), the high sensitivity of β_{DIC} at the high latitudes (Figure 4b), largely driven by temperature, overwhelms the impact of the higher rates of change in C_{ant} in the low latitudes owing to higher buffer capacities (Sabine et al., 2004) (or lower γ_{DIC} , Figure 4c), such that the highest rates of changes in $[H^+]_F$ (pH) are found in the high latitudes. For Ω_{ar} , the situation is reversed. Here the high buffer capacity of the low latitudes (small γ_{DIC} , Figure 4c) with the corresponding higher rates of accumulation of C_{ant} overwhelms the effect of ω_{DIC} , which has the highest (absolute) sensitivity in the high latitudes as well (Figure 4a). The net result is that the highest rates of change in Ω_{ar} occur in the low latitudes. This also means that the highest decreases in Ω_{ar} occur in the regions where Ω_{ar} is highest, while for $[H^+]_F$, the highest increases occur where $[H^+]_F$ is already high, that is, where pH is lowest (Figures 5a and 5d). The former can be largely understood from the fact that the highest rates with which $[CO_3^{2-}]$ is titrated away from the invasion of C_{ant} through the short-circuit reaction $CO_2 + CO_3^{2-} + H_2O = 2HCO_3^-$ (Sarmiento & Gruber, 2006) occurs in the regions where $[CO_3^{2-}]$ is most abundant, that is, where Ω_{ar} is highest. The latter is directly the inverse, that is, the regions where most of the invading C_{ant} is not titrated away but rather stay in its acid form through reaction with water to form H_2CO_3 is where $[CO_3^{2-}]$ (and hence also Ω_{ar}) is the lowest, and where $[H^+]_F$ is highest (or pH lowest).

3.4. Interannual Variability

In addition to the long-term trends, both Ω_{ar} and $[H^+]_F$ are subject to a substantial amount of interannual variability (Figure 5), with Ω_{ar} revealing a much more variable pattern than $[H^+]_F$. The interannual variability for $[H^+]_F$ is primarily confined to the equator, with distinct negative $[H^+]_F$ anomalies found around 1983, 1987, 1992,

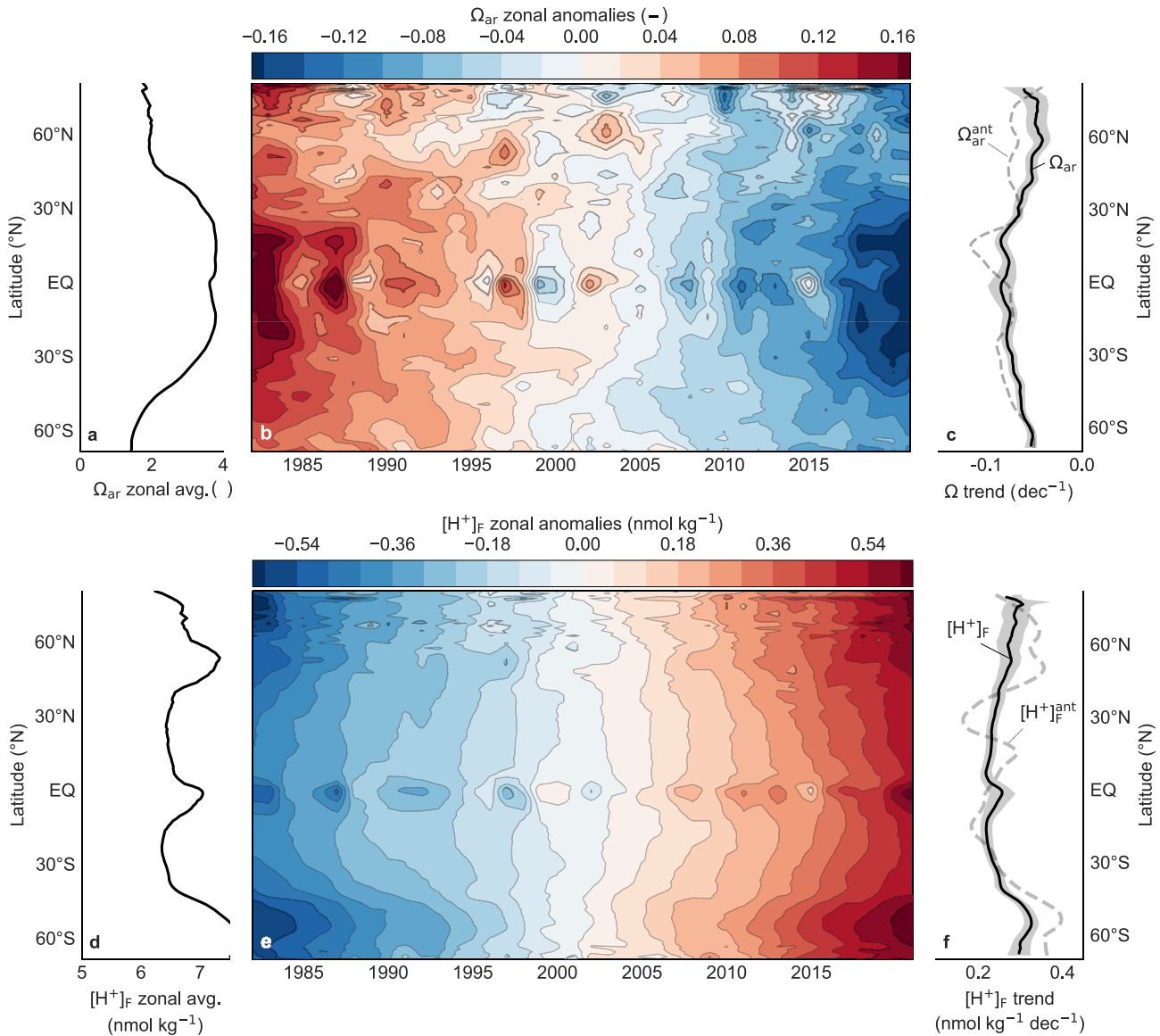


Figure 5. Hovmoeller (latitude-time) diagrams of the zonally averaged anomalies from 1982 through 2021 together with their long-term averages and zonal mean trends. (a) Zonal average of the long-term mean Ω_{ar} . (b) Hovmoeller diagram of the zonally averaged anomalies of Ω_{ar} . The anomalies were computed relative to the long-term mean shown in (a). (c) Zonal average of the long-term linear trend in Ω_{ar} (solid line) together with the trend estimated solely on the basis of the estimated increase in anthropogenic CO_2 (dashed line). (d) As (a), but for $[\text{H}^+]_F$. (e), as (b) but for $[\text{H}^+]_F$. (f), as (c) but for $[\text{H}^+]_F$.

1998, 2002, etc., that is, years characterized by El Niño events in the tropical eastern Pacific. These negative $[\text{H}^+]_F$ anomalies are likely caused by the near cessation of upwelling during these events, thus bringing much less high DIC/low Alk (low $[\text{H}^+]_F$) waters to the surface, keeping surface $[\text{H}^+]_F$ low (and pH high). Even though these events are also characterized by higher than normal sea-surface temperatures, this effect appears to be overwhelmed by the low DIC concentrations that characterize El Niño events (R. Feely et al., 2006; McKinley et al., 2004). Positive anomalies in $[\text{H}^+]_F$ occur during La Niña events, for example, in the years 1988–1989, 1998–1999, 2008–2009, 2010–2011, 2016–2017, when upwelling is strong, bringing large amounts of high DIC/low Alk waters to the surface (Sutton et al., 2014).

The Ω_{ar} anomalies at equatorial latitudes are the opposite of those of $[\text{H}^+]_F$, that is, Ω_{ar} tends to be anomalously high during El Niño events and anomalously low during La Niña events. The drivers are the same as those for $[\text{H}^+]_F$, that is, variations in the strength of upwelling that tend to bring high DIC/low Alk (low Ω_{ar}) waters to the surface.

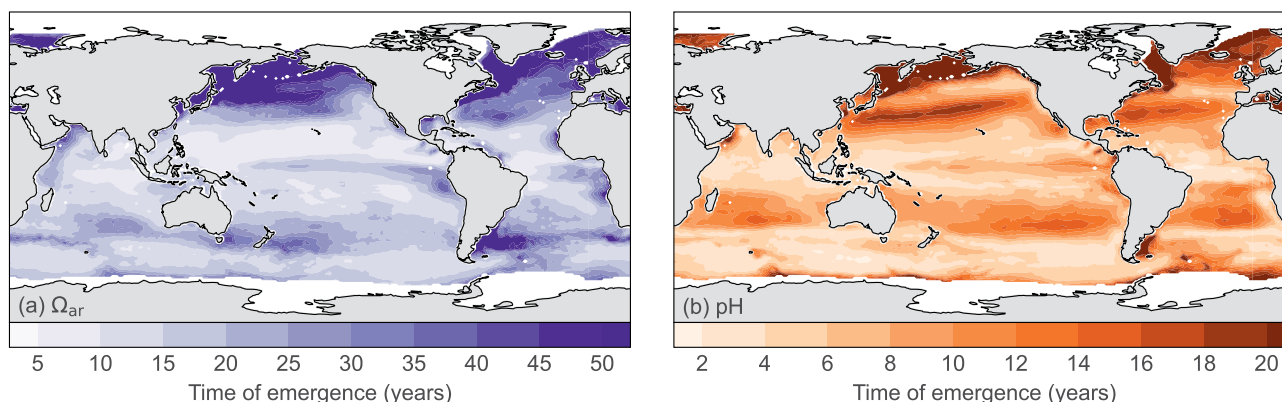


Figure 6. Maps depicting the time of emergence (ToE) for (a) Ω_{ar} and (b) pH. The ToE was estimated from the rates of change in Ω_{ar} and pH and variations in their respective monthly data (including the seasonal cycles), see Equation 5 in the main text.

The Hovmoeller plot for Ω_{ar} reveals also a substantial amount of interannual variability in the extratropics, especially when compared to $[H^+]_F$ (contrast Figure 5b with panel e). The variability in the zonal mean comes from all ocean basins. It is most likely related to the interaction of transport/mixing and biological production that tends to change Ω_{ar} in opposite direction. Their effect is not dampened by co-variations with temperature, since temperature plays a relatively marginal role in controlling Ω_{ar} . This situation tends to differ for $[H^+]_F$, where surface warming/cooling often dampens the effects of transport/mixing and biological production, leading to a relatively low level of spatio-temporal variability (see also Jiang et al. (2019)).

These spatiotemporal variations in Ω_{ar} and in $[H^+]_F$ occur against very different mean concentration gradients (Figures 5a and 5d). The long-term mean of Ω_{ar} varies by more than a factor of 2 across latitudes, with typical values in the high latitudes of around 2, and values of around 4 in the low latitudes (Figure 5a). In contrast, $[H^+]_F$ varies less with latitude, and has, in particular, multiple maxima and minima. Zonal maxima of $[H^+]_F$ occur at the equator and at around 60° in both hemispheres (Figure 5d). $[H^+]_F$ is at its zonal minima in the subtropical gyres and in the Arctic. This difference stems from very different balances controlling the distribution of these two parameters. The distribution of Ω_{ar} is governed by that of the carbonate ion concentration, which is set by the difference between Alk and DIC (Sarmiento & Gruber, 2006). And the latter two parameters are controlled by biology, transport, and mixing, causing strong gradients in space (and time) of DIC and Alk. In contrast, the distribution of pH is very closely related to that of pCO_2 , which is controlled primarily by the interaction with the atmosphere, which tends to equalize the spatial distribution (see discussion in Sarmiento and Gruber (2006)). Since gas exchange is too slow to achieve this equilibrium, gradients remain. Their magnitudes are related to the degree of equilibration versus the degree to which biology, transport, and mixing disturb this equilibrium. These differences in the mean state between Ω_{ar} and in $[H^+]_F$ are then also directly projected into very different levels of variability between the two parameters (Figures 5b and 5e), and also different spatial variations in the trends (Figure 2).

3.5. Time of Emergence

Across the global ocean, the times of emergence (ToE) for both Ω_{ar} and pH estimated from OceanSODA-ETHZ are on the scale of years to decades (Figure 6), with the ToE of pH generally being only half as long as that of Ω_{ar} . The ToE of Ω_{ar} ranges from about 5 years to nearly 50 years, while that of pH ranges from a few years to around 20 years only. In the global weighted mean, the ToE for Ω_{ar} is 25 years, while that for pH is 9 years. This difference is largely a consequence of the higher level of (seasonal) variability in Ω_{ar} compared to that of pH relative to their respective trends.

The longest ToEs are found in the high latitudes of the Northern Hemisphere for both parameters, again largely caused by the high seasonal variations in these regions, but aided, in the case of Ω_{ar} by the small long-term trend in these regions (see Figure 2). Other regions of longer-than-average ToE are the eastern tropical Pacific (owing to strong interannual variability (Figure 5) and a circumpolar band around $40^\circ S$) (owing to high seasonal variability). The ToE of pH has a corresponding band of high ToE in the northern hemisphere, again largely reflecting

the strong seasonal cycle there. A remarkably low ToE is found in the Southern hemisphere, especially for pH, but this is primarily due to the very high trends there (see Figure 2).

Irrespective of the regional variations, the estimated ToEs of less than a few decades imply that over the majority of the surface ocean, the currently observed Ω_{ar} and pH are already outside the variability envelope defined by the data obtained at the beginning of our reconstructions in the early 1980s. This highlights the rapidity of the ongoing OA. This also implies that the development of OA can be easily detected amidst its natural variations in a time frame of a few decades for vast regions of the global oceans.

Our estimate of the ToE compares well with those that have been estimated from models so far (Friedrich et al., 2012; Keller et al., 2014; Rodgers et al., 2015; Schlunegger et al., 2019), although differences in the definition make direct quantifications difficult. For example, Friedrich et al. (2012) used the amplitude of the seasonal cycle as the metric of variance, whereas we use here the standard deviation of the deseasonalized data, that is, we consider primarily the level of interannual variability as the “noise” against which we aim to detect the signal. Schlunegger et al. (2019) and Rodgers et al. (2015) used the “noise” from an ensemble of models and compared that to the trend emerging from the ensemble mean, which is closer to our definition, but still different. Despite these important differences, our work here confirms prior assessments that the signals from OA emerge relatively fast, that is, on the order of years to decades, from the background noise. Our results also confirm prior findings that the equatorial Pacific has one of the longest ToEs (Rodgers et al., 2015). Previously not discussed was the difference between pH and Ω_{ar} , which we are now able to show.

3.6. Caveats and Limitations

We note that the interannual variability of pH, $[H^+]_f$, and Ω_{ar} in the OceanSODA-ETHZ product may be underestimated. We base this potential caveat on the observation that the variability of the pCO₂ data in OceanSODA-ETHZ is on the low end compared to that exhibited in six other surface ocean pCO₂ products (Table S5 in Supporting Information S1). Comparison of zonally averaged interannual variability of pCO₂ between the OceanSODA-ETHZ data set (lowest interannual variability of the seven products) and six other pCO₂-products suggests that the largest discrepancy in their respective interannual variability estimates exists in the high latitudes (Figure S7 in Supporting Information S1). A systematically low interannual variability in the OceanSODA-ETHZ product would directly lead to a systematic underestimation of the ToE. Thus, we conclude that our ToE results may be biased low, although we suspect that this systematic underestimation of the variability would not alter the regional differences. A potential underestimation of the variability would also bias low our trend uncertainties. However, since the trend contribution to the overall uncertainty is relatively small (typically less than 20%), we expect this caveat to have a relatively minor impact on the results.

In addition, we also note that our driver decomposition could be biased since we use the same variables as predictors for generating the fields in the first place and for diagnosing the decomposition in the second place. This is potentially problematic since the predictors are interdependent, especially SST and SSS. While this may not cause problems when predicting the distribution of the variables, it may be problematic when diagnosing the role of freshwater forcing and heating/cooling of the sea surface. We currently do not know how to address this, but we also do not have any evidence that this is an issue. Still, one needs to be aware of this potential caveat when analyzing the driver decomposition.

4. Summary and Conclusions

Our analyses of the OceanSODA-ETHZ product suggest that global surface ocean Ω_{ar} and pH have declined over the past 4 decades at rates of -0.071 ± 0.001 and -0.0166 ± 0.0010 units per decade, respectively. Both trends are predominantly caused by the increase in atmospheric CO₂ driving a trend in the surface ocean concentration of anthropogenic CO₂. Thus, these trends are clearly attributable to human activities, that is, to the anthropogenic emissions of CO₂ by the burning of fossil fuels and land-use change. But we also showed that a decrease in the surface ocean concentration of natural CO₂ and ocean warming modulate the trends measurably. Especially noteworthy is the ~15% enhancement of the pH trend by ocean warming. El Niño and La Niña related variations dominate interannual variability in both Ω_{ar} and pH, with Ω_{ar} varying more strongly. This, together with the stronger seasonal cycle leads to a substantially longer TOE for Ω_{ar} (several decades) compared to pH (around a decade).

Our global trend analyses represent a major step forward relative to prior data-based assessments of the global trends in OA, which were based on a limited number of time series stations (Canadell et al., 2021), based on spatial aggregation of data over large-scale biomes (Lauvset et al., 2015) or using linear regression models only (Iida et al., 2021). Not only were we able to substantially reduce the uncertainties of the trends, but we also pointed out the substantial regional differences in the trends of the most important OA parameters with pH experiencing, on average, the highest rates of changes in the higher latitudes, while the largest changes in Ω_{ar} are found in the tropics. These regional differences need to be taken into account when assessing the impact of OA across the global surface ocean. For example, the especially high rates of change in Ω_{ar} in the eastern Pacific can bring warm-water corals in toward critical saturation thresholds (Hoegh-Guldberg et al., 2007) much faster than inferred from the globally averaged rate of change of Ω_{ar} . Our in situ and satellite observation-based analyses can provide also important evaluation constraints for model studies used to project OA into the future (Kwiatkowski et al., 2020). Of particular concern is again the spatial structure of the simulated changes, an aspect that has not been given a lot of attention so far. Thanks to the near-global coverage of satellite observations that our product is benefitting from, satellite-data-based estimates of OA are especially well positioned to provide the spatiotemporal dimension of OA at the global scale (Land et al., 2019; Shutler et al., 2020).

Understanding the long-term trends and variability of global acidification enables us to put local changes into the larger context of global trends and variability. Even though we emphasized here the role of other drivers, the main driver of OA is the increase in atmospheric CO_2 . Thus, unless the anthropogenic emissions of CO_2 are massively curtailed, OA is bound to continue, increasing its threats on marine life (Bindoff et al., 2019; Kroeker et al., 2013).

Data Availability Statement

All data supporting this work are openly available. The updated version of OceanSODA-ETHZ used here is provided through the National Centers for Environmental Information of NOAA (NCEI) at <https://doi.org/10.25921/m5wx-ja34> (NCEI Accession 0220059) (Gregor & Gruber, 2023). Numerical values of the trends (netCDF) are available through the ETH Research Collection at <https://doi.org/10.3929/ethz-b-000613669> (Ma et al., 2023).

References

- Bakker, D. C. E., Pfeil, B., Landa, C. S., Metzl, N., O'Brien, K. M., Olsen, A., et al. (2016). A multi-decade record of high-quality CO_2 data in version 3 of the Surface Ocean CO_2 Atlas (SOCAT). *Earth System Science Data*, 8(2), 383–413. <https://doi.org/10.5194/essd-8-383-2016>
- Bates, N. R. (2007). Interannual variability of the oceanic CO_2 sink in the subtropical gyre of the North Atlantic Ocean over the last 2 decades. *Journal of Geophysical Research*, 112(C9), C09013. <https://doi.org/10.1029/2006jc003759>
- Bates, N. R., Astor, Y. M., Church, M. J., Currie, K., Dore, J. E., González-Dávila, M., et al. (2014). A time-series view of changing surface ocean chemistry due to ocean uptake of anthropogenic CO_2 and ocean acidification. *Oceanography*, 27(1), 126–141. <https://doi.org/10.5670/oceanog.2014.16>
- Bates, N. R., & Johnson, R. J. (2020). Acceleration of ocean warming, salinification, deoxygenation and acidification in the surface subtropical North Atlantic Ocean. *Communications Earth & Environment*, 1(1), 33. <https://doi.org/10.1038/s43247-020-00030-5>
- Bindoff, N., Cheung, W., Kairo, J., Aristegui, J., Guinder, V., Hallberg, R., et al. (2019). Changing ocean, marine ecosystems, and dependent communities. IPCC special report on the ocean and cryosphere in a changing climate, 477–587. <https://doi.org/10.1017/9781009157964.007>
- Bopp, L., Resplandy, L., Orr, J. C., Doney, S. C., Dunne, J. P., Gehlen, M., et al. (2013). Multiple stressors of ocean ecosystems in the 21st century: Projections with CMIP5 models. *Biogeosciences*, 10(10), 6225–6245. <https://doi.org/10.5194/bg-10-6225-2013>
- Boutin, J., Vergely, J.-L., Marchand, S., d'Amico, F., Hasson, A., Kolodziejczyk, N., et al. (2018). New SMOS sea surface salinity with reduced systematic errors and improved variability. *Remote Sensing of Environment*, 214, 115–134. <https://doi.org/10.1016/j.rse.2018.05.022>
- Boyer, T. P., Garcia, H. E., Locarnini, R. A., Zweng, M. M., Mishonov, A. V., Reagan, J. R., et al. (2018). *World Ocean Atlas 2018*. NOAA National Centers for Environmental Information.
- Brewer, P. G. (2013). A short history of ocean acidification science in the 20th century: A chemist's view. *Biogeosciences*, 10(11), 7411–7422. <https://doi.org/10.5194/bg-10-7411-2013>
- Byrne, R. H., & Breland, J. A. (1989). High precision multiwavelength pH determinations in seawater using cresol red. *Deep Sea Research Part A. Oceanographic Research Papers*, 36(5), 803–810. [https://doi.org/10.1016/0198-0149\(89\)90152-0](https://doi.org/10.1016/0198-0149(89)90152-0)
- Byrne, R. H., & Yao, W. (2008). Procedures for measurement of carbonate ion concentrations in seawater by direct spectrophotometric observations of Pb(II) complexation. *Marine Chemistry*, 112(1–2), 128–135. <https://doi.org/10.1016/j.marchem.2008.07.009>
- Caldeira, K., & Wickett, M. E. (2003). Anthropogenic carbon and ocean pH. *Nature*, 425(6956), 365. <https://doi.org/10.1038/425365a>
- Canadell, P., Monteiro, P., Costa, M., da Cunha, L. C., Cox, P., Eliseev, A., et al. (2021). Global carbon and other biogeochemical cycles and feedbacks. In *Climate change 2021: The physical science basis. Contribution of working group I to the sixth assessment report of the intergovernmental panel on climate change* (pp. 673–816). <https://doi.org/10.1017/9781009157896.007>
- Carton, J. A., Chepurin, G. A., & Chen, L. (2018). SODA3: A new ocean climate reanalysis. *Journal of Climate*, 31(17), 6967–6983. <https://doi.org/10.1175/jcli-d-18-0149.1>
- Chau, T. T., Gehlen, M., & Chevallier, F. (2022). A seamless ensemble-based reconstruction of surface ocean pCO_2 and air–sea CO_2 fluxes over the global coastal and open oceans. *Biogeosciences*, 19(4), 1087–1109. <https://doi.org/10.5194/bg-19-1087-2022>

Acknowledgments

This research was supported by the European Space Agency (OceanSODA project, Grant 4000112091/14/I-LG, Ocean Health Ocean Acidification project, Grant AO/1-10757/21/I-DT), and by the European Commission through its Horizon 2020 research and innovation programme under Grant agreements no. 821003 (project 4C) and no. 820989 (COMFORT). Open access funding provided by Eidgenössische Technische Hochschule Zurich.

- Claustre, H., Johnson, K. S., & Takeshita, Y. (2020). Observing the global ocean with biogeochemical-argo. *Annual Review of Marine Science*, 12(1), 23–48. <https://doi.org/10.1146/annurev-marine-010419-010956>
- Clayton, T. D., & Byrne, R. H. (1993). Spectrophotometric seawater pH measurements: Total hydrogen ion concentration scale calibration of m-cresol purple and at-sea results. *Deep Sea Research Part I: Oceanographic Research Papers*, 40(10), 2115–2129. [https://doi.org/10.1016/0967-0637\(93\)90048-8](https://doi.org/10.1016/0967-0637(93)90048-8)
- Clement, D., & Gruber, N. (2018). The eMLR(C*) method to determine decadal changes in the global ocean storage of anthropogenic CO₂. *Global Biogeochemical Cycles*, 32(4), 654–679. <https://doi.org/10.1002/2017GB005819>
- Cornwall, C. E., Comeau, S., Kornder, N. A., Perry, C. T., van Hooijdonk, R., DeCarlo, T. M., et al. (2021). Global declines in coral reef calcium carbonate production under ocean acidification and warming. *Proceedings of the National Academy of Sciences of the United States*, 118(21). <https://doi.org/10.1073/pnas.2015265118>
- Cornwall, C. E., Harvey, B. P., Comeau, S., Cornwall, D. L., Hall-Spencer, J. M., Peña, V., et al. (2022). Understanding coralline algal responses to ocean acidification: Meta-analysis and synthesis. *Global Change Biology*, 28(2), 362–374. <https://doi.org/10.1111/gcb.15899>
- DeVries, T. (2014). The oceanic anthropogenic CO₂ sink: Storage, air-sea fluxes, and transports over the industrial era. *Global Biogeochemical Cycles*, 28(7), 631–647. <https://doi.org/10.1002/2013gb004739>
- Dickson, A. G., Sabine, C. L., & Christian, J. R. (2007). Guide to best practices for ocean CO₂ measurements (Vol. 3).
- Dickson, A. G. (1993). The measurement of seawater pH. *Marine Chemistry*, 44(2–4), 131–142. [https://doi.org/10.1016/0304-4203\(93\)90198-w](https://doi.org/10.1016/0304-4203(93)90198-w)
- Dickson, A. G., & Millero, F. J. (1987). A comparison of the equilibrium constants for the dissociation of carbonic acid in seawater media. *Deep Sea Research Part A. Oceanographic Research Papers*, 34(10), 1733–1743. [https://doi.org/10.1016/0198-0149\(87\)90021-5](https://doi.org/10.1016/0198-0149(87)90021-5)
- Dickson, A. G., Wesolowski, D. J., Palmer, D. A., & Mesmer, R. E. (1990). Dissociation constant of bisulfate ion in aqueous sodium chloride solutions to 250°C. *Journal of Physical Chemistry*, 94(20), 7978–7985. <https://doi.org/10.1021/j100383a042>
- Dlugokencky, E., Thoning, K., Lan, X., & Tans, P. (2021). NOAA greenhouse gas reference from atmospheric carbon dioxide dry air mole fractions from the NOAA GML carbon cycle cooperative global air sampling network. <https://doi.org/10.15138/9N0H-ZH07>
- Doney, S. C., Busch, D. S., Cooley, S. R., & Kroeker, K. J. (2020). The impacts of ocean acidification on marine ecosystems and reliant human communities. *Annual Review of Environment and Resources*, 45(1), 83–112. <https://doi.org/10.1146/annurev-environ-012320-083019>
- Doney, S. C., Fabry, V. J., Feely, R. A., & Kleypas, J. A. (2009). Ocean acidification: The other CO₂ problem. *Annual Review of Marine Science*, 1, 169–192. <https://doi.org/10.1146/annurev.marine.010908.163834>
- Dore, J. E., Lukas, R., Sadler, D. W., Church, M. J., & Karl, D. M. (2009). Physical and biogeochemical modulation of ocean acidification in the central North Pacific. *Proceedings of the National Academy of Sciences of the United States of America*, 106(30), 12235–12240. <https://doi.org/10.1073/pnas.0906044106>
- Egleston, E. S., Sabine, C. L., & Morel, F. M. (2010). Revelle revisited: Buffer factors that quantify the response of ocean chemistry to changes in DIC and alkalinity. *Global Biogeochemical Cycles*, 24(1). <https://doi.org/10.1029/2008gb003407>
- Fay, A. R., Gregor, L., Landschützer, P., McKinley, G. A., Gruber, N., Gehlen, M., et al. (2021). SeaFlux: Harmonization of air–sea CO₂ fluxes from surface pCO₂ data products using a standardized approach. *Earth System Science Data*, 13(10), 4693–4710. <https://doi.org/10.5194/essd-13-4693-2021>
- Fay, A. R., & McKinley, G. A. (2013). Global trends in surface ocean pCO₂ from in situ data. *Global Biogeochemical Cycles*, 27(2), 541–557. <https://doi.org/10.1002/gbc.20051>
- Fay, A. R., & McKinley, G. A. (2014). Global open-ocean biomes: Mean and temporal variability. *Earth System Science Data*, 6(2), 273–284. <https://doi.org/10.5194/essd-6-273-2014>
- Feely, R., Takahashi, T., Wanninkhof, R., McPhaden, M., Cosca, C., Sutherland, S., & Carr, M.-E. (2006). Decadal variability of the air-sea CO₂ fluxes in the equatorial Pacific Ocean. *Journal of Geophysical Research*, 111(C8), C08S90. <https://doi.org/10.1029/2005jc003129>
- Feely, R. A., Doney, S. C., & Cooley, S. R. (2009). Ocean acidification: Present conditions and future changes in a high-CO₂ world. *Oceanography*, 22(4), 36–47. <https://doi.org/10.5670/oceanog.2009.95>
- Feely, R. A., Sabine, C. L., Lee, K., Berelson, W., Kleypas, J., Fabry, V. J., & Millero, F. J. (2004). Impact of anthropogenic CO₂ on the CaCO₃ system in the oceans. *Science*, 305(5682), 362–366. <https://doi.org/10.1126/science.1097329>
- Figuerola, B., Hancock, A. M., Bax, N., Cummings, V. J., Downey, R., Griffiths, H. J., et al. (2021). A review and meta-analysis of potential impacts of ocean acidification on marine calcifiers from the Southern Ocean. *Frontiers in Marine Science*, 8, 24. <https://doi.org/10.3389/fmars.2021.584445>
- Friedlingstein, P., Jones, M. W., O’Sullivan, M., Andrew, R. M., Bakker, D. C. E., Hauck, J., et al. (2022). Global carbon budget 2021. *Earth System Science Data*, 14(4), 1917–2005. <https://doi.org/10.5194/essd-14-1917-2022>
- Friedrich, T., Timmermann, A., Abe-Ouchi, A., Bates, N., Chikamoto, M., Church, M., et al. (2012). Detecting regional anthropogenic trends in ocean acidification against natural variability. *Nature Climate Change*, 2(3), 167–171. <https://doi.org/10.1038/nclimate1372>
- Gloege, L., Yan, M., Zheng, T., & McKinley, G. A. (2022). Improved quantification of ocean carbon uptake by using machine learning to merge global models and pCO₂ data. *Journal of Advances in Modeling Earth Systems*, 14(2), e2021MS002620. <https://doi.org/10.1029/2021ms002620>
- Gregor, L., & Gruber, N. (2021). OceanSODA-ETHZ: A global gridded data set of the surface ocean carbonate system for seasonal to decadal studies of ocean acidification. *Earth System Science Data*, 13(2), 777–808. <https://doi.org/10.5194/essd-13-777-2021>
- Gregor, L., & Gruber, N. (2023). OceanSODA-ETHZ: A global gridded dataset of the surface ocean carbonate system for seasonal to decadal studies of ocean acidification (v2022) (NCEI accession 0220059) [Dataset]. NOAA National Centers for Environmental Information. <https://doi.org/10.25921/m5wx-ja34>
- Gruber, N., Bakker, D. C., DeVries, T., Gregor, L., Hauck, J., Landschützer, P., et al. (2023). Trends and variability in the ocean carbon sink. *Nature Reviews Earth & Environment*, 4(2), 1–16. <https://doi.org/10.1038/s43017-022-00381-x>
- Gruber, N., Bates, N. R., & Keeling, C. D. (2002). Interannual variability in the North Atlantic carbon sink. *Science*, 298(5602), 2374–2378. <https://doi.org/10.1126/science.1077077>
- Gruber, N., Clement, D., Carter, B. R., Feely, R. A., van Heuven, S., Hoppema, M., et al. (2019). The oceanic sink for anthropogenic CO₂ from 1994 to 2007. *Science*, 363(6432), 1193–1199. <https://doi.org/10.1126/science.aau5153>
- Gruber, N., Hauri, C., Lachkar, Z., Loher, D., Frölicher, T. L., & Plattner, G.-K. (2012). Rapid progression of ocean acidification in the California Current System. *Science*, 337(6091), 220–223. <https://doi.org/10.1126/science.1216773>
- Hall-Spencer, J. M., & Harvey, B. P. (2019). Ocean acidification impacts on coastal ecosystem services due to habitat degradation. *Emerging Topics in Life Sciences*, 3(2), 197–206. <https://doi.org/10.1042/etls20180117>
- Harvey, B. P., Kon, K., Agostini, S., Wada, S., & Hall-Spencer, J. M. (2021). Ocean acidification locks algal communities in a species-poor early successional stage. *Global Change Biology*, 27(10), 2174–2187. <https://doi.org/10.1111/gcb.15455>
- Hauck, J., Zeising, M., Le Quéré, C., Gruber, N., Bakker, D. C. E., Bopp, L., et al. (2020). Consistency and challenges in the ocean carbon sink estimate for the global carbon budget. *Frontiers in Marine Science*, 7, 1–33. <https://doi.org/10.3389/fmars.2020.571720>

- Hoegh-Guldberg, O., Mumby, P. J., Hooten, A. J., Steneck, R. S., Greenfield, P., Gomez, E., et al. (2007). Coral reefs under rapid climate change and ocean acidification. *Science*, *318*(5857), 1737–1742. <https://doi.org/10.1126/science.1152509>
- Humphreys, M. P., Gregor, L., Pierrot, D., van Heuven, S., Lewis, E. R., & Wallace, D. W. (2020). PyCO2SYS: Marine carbonate system calculations in python. <https://doi.org/10.5281/ZENODO.3967359>
- Iida, Y., Takatani, Y., Kojima, A., & Ishii, M. (2021). Global trends of ocean CO₂ sink and ocean acidification: An observation-based reconstruction of surface ocean inorganic carbon variables. *Journal of Oceanography*, *77*(2), 323–358. <https://doi.org/10.1007/s10872-020-00571-5>
- Ishii, M., Rodgers, K. B., Inoue, H. Y., Toyama, K., Sasano, D., Kosugi, N., et al. (2020). Ocean acidification from below in the tropical Pacific. *Global Biogeochemical Cycles*, *34*(8), e2019GB006368. <https://doi.org/10.1029/2019gb006368>
- Jiang, L.-Q., Carter, B. R., Feely, R. A., Lauvset, S. K., & Olsen, A. (2019). Surface ocean pH and buffer capacity: Past, present and future. *Scientific Reports*, *9*(1), 1–11. <https://doi.org/10.1038/s41598-019-55039-4>
- Johnson, G. C., & Lyman, J. M. (2020). Warming trends increasingly dominate global ocean. *Nature Climate Change*, *10*(8), 757–761. <https://doi.org/10.1038/s41558-020-0822-0>
- Keller, K. M., Joos, F., & Raible, C. C. (2014). Time of emergence of trends in ocean biogeochemistry. *Biogeosciences*, *11*(13), 3647–3659. <https://doi.org/10.5194/bg-11-3647-2014>
- Keppler, L., Landschützer, P., Lauvset, S. K., & Gruber, N. (2023). Recent trends and variability in the oceanic storage of dissolved inorganic carbon. *Global Biogeochemical Cycles*, *37*(5). <https://doi.org/10.1029/2022GB007677>
- Khatiwalala, S., Tanhua, T., Mikaloff Fletcher, S., Gerber, M., Doney, S. C., Graven, H. D., et al. (2013). Global ocean storage of anthropogenic carbon. *Biogeosciences*, *10*(4), 2169–2191. <https://doi.org/10.5194/bg-10-2169-2013>
- Kim, J.-Y., Kang, D.-J., Lee, T., & Kim, K.-R. (2014). Long-term trend of CO₂ and ocean acidification in the surface water of the Ulleung Basin, the East Japan Sea inferred from the underway observational data. *Biogeosciences*, *11*(9), 2443–2454. <https://doi.org/10.5194/bg-11-2443-2014>
- Kroeker, K. J., Kordas, R. L., Crim, R., Hendriks, I. E., Ramajo, L., Singh, G. S., et al. (2013). Impacts of ocean acidification on marine organisms: Quantifying sensitivities and interaction with warming. *Global Change Biology*, *19*(6), 1884–1896. <https://doi.org/10.1111/gcb.12179>
- Kwiatkowski, L., Torres, O., Bopp, L., Aumont, O., Chamberlain, M., Christian, J. R., et al. (2020). Twenty-first century ocean warming, acidification, deoxygenation, and upper-ocean nutrient and primary production decline from CMIP6 model projections. *Biogeosciences*, *17*(13), 3439–3470. <https://doi.org/10.5194/bg-17-3439-2020>
- Land, P. E., Findlay, H. S., Shutler, J. D., Ashton, I. G., Holding, T., Grouazel, A., et al. (2019). Optimum satellite remote sensing of the marine carbonate system using empirical algorithms in the global ocean, the Greater Caribbean, the Amazon Plume and the Bay of Bengal. *Remote Sensing of Environment*, *235*, 111469. <https://doi.org/10.1016/j.rse.2019.111469>
- Landschützer, P., Gruber, N., & Bakker, D. C. (2016). Decadal variations and trends of the global ocean carbon sink. *Global Biogeochemical Cycles*, *30*(10), 1396–1417. <https://doi.org/10.1002/2015gb005359>
- Landschützer, P., Gruber, N., Bakker, D. C., & Schuster, U. (2014). Recent variability of the global ocean carbon sink. *Global Biogeochemical Cycles*, *28*(9), 927–949. <https://doi.org/10.1002/2014gb004853>
- Landschützer, P., Gruber, N., Bakker, D. C., Stemmler, I., & Six, K. D. (2018). Strengthening seasonal marine CO₂ variations due to increasing atmospheric CO₂. *Nature Climate Change*, *8*(2), 146–150. <https://doi.org/10.1038/s41558-017-0057-x>
- Lauvset, S. K., & Gruber, N. (2014). Long-term trends in surface ocean pH in the north Atlantic. *Marine Chemistry*, *162*, 71–76. <https://doi.org/10.1016/j.marchem.2014.03.009>
- Lauvset, S. K., Gruber, N., Landschützer, P., Olsen, A., & Tjiputra, J. (2015). Trends and drivers in global surface ocean pH over the past 3 decades. *Biogeosciences*, *12*(5), 1285–1298. <https://doi.org/10.5194/bg-12-1285-2015>
- Leseurre, C., Monaco, C. L., Reverdin, G., Metzl, N., Fin, J., Mignon, C., & Benito, L. (2022). Trends and drivers of sea surface fCO₂ and pH changes observed in the Southern Indian Ocean over the last two decades (1998–2019). *Biogeosciences*, *19*(10), 2599–2625. <https://doi.org/10.5194/bg-19-2599-2022>
- Lewis, E., Wallace, D., & Allison, L. J. (1998). *Program developed for CO₂ system calculations*. (Technical Report). Oak Ridge, TN 37831-6335. Brookhaven National Laboratory, Department of Applied Science.
- Lovenduski, N. S., Gruber, N., Doney, S. C., & Lima, I. D. (2007). Enhanced CO₂ outgassing in the Southern Ocean from a positive phase of the Southern Annular Mode. *Global Biogeochemical Cycles*, *21*(2). <https://doi.org/10.1029/2006gb002900>
- Ma, D., Gregor, L., & Gruber, N. (2023). Data of trends and drivers of global surface ocean acidification over the past four decades [Dataset]. ETH Zurich. <https://doi.org/10.3929/ethz-b-000613669>
- Matsumoto, K., & Gruber, N. (2005). How accurate is the estimation of anthropogenic carbon in the ocean? An evaluation of the ΔC* method. *Global Biogeochemical Cycles*, *19*(3). <https://doi.org/10.1029/2004gb002397>
- McKinley, G. A., Follows, M. J., & Marshall, J. (2004). Mechanisms of air-sea CO₂ flux variability in the equatorial Pacific and the North Atlantic. *Global Biogeochemical Cycles*, *18*(2). <https://doi.org/10.1029/2003gb002179>
- McNeil, B., & Matear, R. (2013). The non-steady state oceanic CO₂ signal: Its importance, magnitude and a novel way to detect it. *Biogeosciences*, *10*(4), 2219–2228. <https://doi.org/10.5194/bg-10-2219-2013>
- Mehrbach, C., Culbertson, C., Hawley, J., & Pytkowicz, R. (1973). Measurement of the apparent dissociation constants of carbonic acid in seawater at atmospheric pressure 1. *Limnology & Oceanography*, *18*(6), 897–907. <https://doi.org/10.4319/lo.1973.18.6.0897>
- Mikaloff Fletcher, S. E., Gruber, N., Jacobson, A. R., Doney, S. C., Dutkiewicz, S., Gerber, M., et al. (2006). Inverse estimates of anthropogenic CO₂ uptake, transport, and storage by the ocean. *Global Biogeochemical Cycles*, *20*(2). <https://doi.org/10.1029/2005gb002530>
- Mucci, A. (1983). The solubility of calcite and aragonite in seawater at various salinities, temperatures, and one atmosphere total pressure. *American Journal of Science*, *283*(7), 780–799. <https://doi.org/10.2475/ajs.283.7.780>
- Olafsson, J., Olafsdottir, S., Benoit-Cattin, A., & Takahashi, T. (2010). The Irminger Sea and the Iceland Sea time series measurements of sea water carbon and nutrient chemistry 1983–2008. *Earth System Science Data*, *2*(1), 99–104. <https://doi.org/10.5194/essd-2-99-2010>
- Olsen, A., Key, R. M., van Heuven, S., Lauvset, S. K., Velo, A., Lin, X., et al. (2016). The Global Ocean Data Analysis Project version 2 (GLODAPv2)—An internally consistent data product for the world ocean. *Earth System Science Data*, *8*(2), 297–323. <https://doi.org/10.5194/essd-8-297-2016>
- Orr, J. C. (2011). *Recent and future changes in ocean carbonate chemistry*. (Vol. 1, pp. 41–66). Oxford University Press.
- Orr, J. C., Fabry, V. J., Aumont, O., Bopp, L., Doney, S. C., Feely, R. A., et al. (2005). Anthropogenic ocean acidification over the twenty-first century and its impact on calcifying organisms. *Nature*, *437*(7059), 681–686. <https://doi.org/10.1038/nature04095>
- Radford, C., Collins, S., Munday, P., & Parsons, D. (2021). Ocean acidification effects on fish hearing. *Proceedings of the Royal Society B*, *288*(1946), 20202754. <https://doi.org/10.1098/rspb.2020.2754>
- Raimondi, L., Matthews, J. B. R., Atamanchuk, D., Azetsu-Scott, K., & Wallace, D. W. (2019). The internal consistency of the marine carbon dioxide system for high latitude shipboard and in situ monitoring. *Marine Chemistry*, *213*, 49–70. <https://doi.org/10.1016/j.marchem.2019.03.001>

- Reynolds, R. W., Smith, T. M., Liu, C., Chelton, D. B., Casey, K. S., & Schlax, M. G. (2007). Daily high-resolution-blended analyses for sea surface temperature. *Journal of Climate*, *20*(22), 5473–5496. <https://doi.org/10.1175/2007jcli1824.1>
- Rödenbeck, C., Bakker, D. C. E., Gruber, N., Iida, Y., Jacobson, A. R., Jones, S. D., et al. (2015). Data-based estimates of the ocean carbon sink variability—first results of the Surface Ocean pCO₂ Mapping intercomparison (SOCOM). *Biogeosciences*, *12*(23), 7251–7278. <https://doi.org/10.5194/bg-12-7251-2015>
- Rodgers, K. B., Lin, J., & Frölicher, T. L. (2015). Emergence of multiple ocean ecosystem drivers in a large ensemble suite with an Earth system model. *Biogeosciences*, *12*(11), 3301–3320. <https://doi.org/10.5194/bg-12-3301-2015>
- Sabine, C. L., Feely, R. A., Gruber, N., Key, R. M., Lee, K., Bullister, J. L., et al. (2004). The oceanic sink for anthropogenic CO₂. *Science*, *305*(5682), 367–371. <https://doi.org/10.1126/science.1097403>
- Sallée, J.-B., Pellichero, V., Akhoudas, C., Pauthenet, E., Vignes, L., Schmidt, S., et al. (2021). Summertime increases in upper-ocean stratification and mixed-layer depth. *Nature*, *591*(7851), 592–598. <https://doi.org/10.1038/s41586-021-03303-x>
- Sarmiento, J., & Gruber, N. (2006). *Ocean biogeochemical dynamics*. Princeton University Press.
- Schlunegger, S., Rodgers, K. B., Sarmiento, J. L., Frölicher, T. L., Dunne, J. P., Ishii, M., & Slater, R. (2019). Emergence of anthropogenic signals in the ocean carbon cycle. *Nature Climate Change*, *9*(9), 719–725. <https://doi.org/10.1038/s41558-019-0553-2>
- Shutler, J. D., Wanninkhof, R., Nightingale, P. D., Woolf, D. K., Bakker, D. C., Watson, A., et al. (2020). Satellites will address critical science priorities for quantifying ocean carbon. *Frontiers in Ecology and the Environment*, *18*(1), 27–35. <https://doi.org/10.1002/fee.2129>
- Sutton, A. J., Feely, R. A., Sabine, C. L., McPhaden, M. J., Takahashi, T., Chavez, F. P., et al. (2014). Natural variability and anthropogenic change in equatorial Pacific surface ocean pCO₂ and pH. *Global Biogeochemical Cycles*, *28*(2), 131–145. <https://doi.org/10.1002/2013gb004679>
- Takahashi, T., Sutherland, S. C., Chipman, D. W., Goddard, J. G., Ho, C., Newberger, T., et al. (2014). Climatological distributions of pH, pCO₂, total CO₂, alkalinity, and CaCO₃ saturation in the global surface ocean, and temporal changes at selected locations. *Marine Chemistry*, *164*, 95–125. <https://doi.org/10.1016/j.marchem.2014.06.004>
- Terhaar, J., Frölicher, T. L., & Joos, F. (2023). Ocean acidification in emission-driven temperature stabilization scenarios: The role of TCRE and non-CO₂ greenhouse gases. *Environmental Research Letters*, *18*(2), 024033. <https://doi.org/10.1088/1748-9326/acaf91>
- Tilbrook, B., Jewett, E. B., DeGrandpre, M. D., Hernandez-Ayon, J. M., Feely, R. A., Gledhill, D. K., et al. (2019). An enhanced ocean acidification observing network: From people to technology to data synthesis and information exchange. *Frontiers in Marine Science*, *337*. <https://doi.org/10.3389/fmars.2019.00337>
- Tjiputra, J. F., Olsen, A., Bopp, L., Lenton, A., Pfeil, B., Roy, T., et al. (2014). Long-term surface pCO₂ trends from observations and models. *Tellus B: Chemical and Physical Meteorology*, *66*(1), 23083. <https://doi.org/10.3402/tellusb.v66.23083>
- Uppström, L. R. (1974). The boron/chlorinity ratio of deep-sea water from the Pacific Ocean. *Deep-Sea Research and Oceanographic Abstracts*, *21*(2), 161–162. [https://doi.org/10.1016/0011-7471\(74\)90074-6](https://doi.org/10.1016/0011-7471(74)90074-6)
- Weiss, R. (1974). Carbon dioxide in water and seawater: The solubility of non-ideal gas. *Marine Chemistry*, *2*(3), 203–215. [https://doi.org/10.1016/0304-4203\(74\)90015-2](https://doi.org/10.1016/0304-4203(74)90015-2)